Expert recommendations on the assessment of wall shear stress in human coronary arteries: existing methodologies, technical considerations, and clinical applications

As Published: 10.1093/EURHEARTJ/EHZ551

Publisher: Oxford University Press (OUP)

Persistent URL: https://hdl.handle.net/1721.1/136416

Version: Final published version: final published article, as it appeared in a journal, conference proceedings, or other formally published context

ESC European Society of Cardiology

European Heart Journal (2019) **40**, 3421–3433
doi:10.1093/eurheartj/ehz551

Expert recommendations on the assessment of wall shear stress in human coronary arteries: existing methodologies, technical considerations, and clinical applications

Frank Gijsen [1], Yuki Katagiri[2], Peter Barlis[3,4,5], Christos Bourantas[6,7,8], Carlos Collet[2], Umit Coskun[9], Joost Daemen [1], Jouke Dijkstra[10], Elazer Edelman [9,11], Paul Evans[12], Kim van der Heiden [1], Rod Hose[12,13], Bon-Kwon Koo [14,15], Rob Krams [16], Alison Marsden[17], Francesco Migliavacca [18], Yoshinobu Onuma[19], Andrew Ooi [20], Eric Poon [20], Habib Samady[21], Peter Stone[9], Kuniaki Takahashi [2], Dalin Tang[22], Vikas Thondapu [20,23,24], Erhan Tenekecioglu[25], Lucas Timmins [26,27], Ryo Torii [28], Jolanda Wentzel [1], and Patrick Serruys [19,29,30]

[1]Department of Cardiology, Erasmus MC, University Medical Center Rotterdam, Rotterdam, the Netherlands; [2]Amsterdam University Medical Centre, University of Amsterdam, Amsterdam, the Netherlands; [3]Department of Medicine and Radiology, Melbourne Medical School, Faculty of Medicine, Dentistry and Health Sciences, The University of Melbourne, Melbourne, VIC, Australia; [4]Department of Cardiology, Northern Hospital, 185 Cooper Street, Epping, Australia; [5]St Vincent's Heart Centre, Building C, 41 Victoria Parade, Fitzroy, Australia; [6]Institute of Cardiovascular Sciences, University College of London, London, UK; [7]Department of Cardiology, Barts Heart Centre, London, UK; [8]School of Medicine and Dentistry, Queen Mary University London, London, UK; [9]Division of Cardiovascular Medicine, Brigham & Women's Hospital, Harvard Medical School, Boston, MA, USA; [10]LKEB-Division of Image Processing, Department of Radiology, Leiden University Medical Centre, Leiden, the Netherlands; [11]Institute for Medical Engineering and Science, MIT, Cambridge, MA, USA; [12]Department of Infection, Immunity and Cardiovascular Disease, University of Sheffield, UK; [13]Department of Circulation and Imaging, NTNU, Trondheim, Norway; [14]Department of Internal Medicine and Cardiovascular Center, Seoul National University Hospital, Seoul, Korea; [15]Institute of Aging, Seoul National University, Seoul, Korea; [16]School of Engineering and Materials Science Queen Mary University of London, London, UK; [17]Departments of Bioengineering and Pediatrics, Institute of Computational and Mathematical Engineering, Stanford University, Stanford, CA, USA; [18]Laboratory of Biological Structure Mechanics (LaBS), Department of Chemistry, Materials and Chemical Engineering "Giulio Natta", Politecnico di Milano, Milan, Italy; [19]Erasmus University Medical Center, Rotterdam, the Netherlands; [20]Department of Mechanical Engineering, Melbourne School of Engineering, The University of Melbourne, Melbourne, VIC, Australia; [21]Department of Medicine, Emory University School of Medicine, Atlanta, GA, USA; [22]Department of Mathematics, Southeast University, Nanjing, China; Mathematical Sciences Department, Worcester Polytechnic Institute, Worcester, MA, USA; [23]Department of Medicine and Radiology, Melbourne Medical School, Faculty of Medicine, Dentistry and Health Sciences, The University of Melbourne, Melbourne, VIC, Australia; [24]Cardiology Division, Massachusetts General Hospital, Harvard Medical School, Boston, MA, USA; [25]Department of Interventional Cardiology, Thoraxcentre, Erasmus Medical Centre, Rotterdam, the Netherlands; [26]Department of Biomedical Engineering, University of Utah, Salt Lake City, UT; [27]Scientific Computing and Imaging Institute, University of Utah, Salt Lake City, UT; [28]Department of Mechanical Engineering, University College London, UK; [29]Imperial College London, London, UK; and [30]Melbourne School of Engineering, University of Melbourne, Melbourne, Australia

Received 19 December 2018; revised 9 April 2019; editorial decision 7 July 2019; accepted 23 September 2019; online publish-ahead-of-print 30 September 2019

Introduction

What is wall shear stress?

When blood flows through an artery, it exerts forces on the vessel wall (*Figure 1*). The perpendicular component of that force vector is associated with blood pressure, leading to deformation of the cells in the vessel wall. The tangential component of that force vector is much smaller and can be sensed by the endothelium through a shearing deformation ('shearing force'). Each force has a magnitude and direction, and for the shear force, they both change during the cardiac cycle. If we normalize this tangential force vector by the area, we obtain the wall shear stress (unit: 1 Pa = 10 dynes/cm^2). Wall shear stress has a major impact on endothelial function and therefore plays a key role in atherosclerotic disease development and in long-term evolution and healing of vessels treated by intravascular devices. Wall shear stress is orders of magnitude smaller than other mechanical stresses affecting the coronary arteries, such as tensile stress or compressive stress and exerts its powerful vascular effects not by a mechanical impact on vascular structure per se, but uniquely by triggering biologic signalling. The biological impact of wall shear stress will be reviewed briefly in 'The biological relevance of wall shear stress' section.

* Corresponding author. Tel: 31-102062828, Email: patrick.w.j.c.serruys@gmail.com

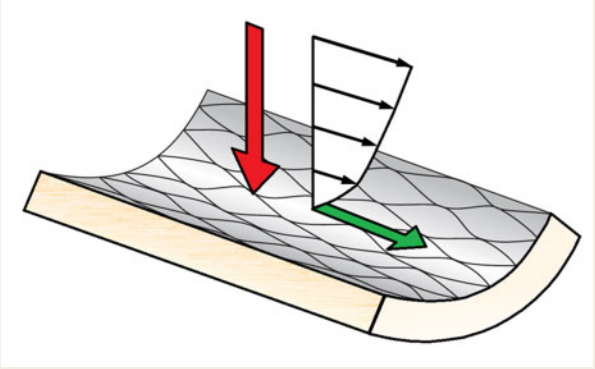

Figure 1 A schematic representation of the forces the vessel wall is exposed to. The red arrow is the normal force component, associated with blood pressure, and the green arrow is the tangential component force, associated with wall shear stress. Note that the size of the arrows does not represents the magnitude of the forces, only the direction.

How do we calculate wall shear stress?

Since wall shear stress in coronary arteries cannot be measured directly, we need to compute through solving the equations that describe the motion of fluids: the Navier–Stokes equations. The most widely used method to solve these complex equations is called computational fluid dynamics (CFD). Given the appropriate input data, the velocity and pressure distribution can be computed with CFD and the local wall shear stress distribution in coronary arteries can be derived. CFD in the coronary arteries has recently gained increased clinical interest with the advent of computed tomography coronary angiography-derived fractional flow reserve (FFR_{CT}) technology for non-invasive assessment of coronary stenosis severity.

The solution of the full Navier–Stokes equations provides complete velocity and pressure information at *any* location in the coronary artery at *any* point in time. Solving these equations can be time consuming and computationally expensive and therefore many studies make use of simplified equations, many of them building on the seminal work of Young and Tsai and Gould.[1–3] Reductional approaches can be useful for specialized applications, but they often rely on assumptions that do not hold for coronary artery flow. A recent series of applications produce predictions of bulk pressure drops in stenosed arteries under hyperaemia to determine the FFR. Especially under elevated flow conditions, the non-linear nature of the Navier–Stokes equations becomes dominant, often leading to an underestimation of the pressure drop when applying reduced models.

Aim and outline

The aim of this manuscript is to provide guidelines for appropriate use of CFD to obtain reproducible and reliable wall shear stress maps in native and instrumented human coronary arteries. The outcome of CFD heavily depends on the quality of the input data, which include vessel geometrical data, proper boundary conditions, and material models. Available methodologies to reconstruct coronary artery anatomy are discussed in 'Imaging coronary arteries: a brief review' section. Computational procedures implemented to simulate blood flow in native coronary arteries are presented in 'Wall shear stress in native arteries' section. The effect of including different geometrical scales due to the presence of stent struts in instrumented arteries is highlighted in 'Wall shear stress in stents' section. The clinical implications are discussed in 'Clinical applications' section, and concluding remarks are presented in 'Concluding remarks' section.

The biological relevance of wall shear stress

Wall shear stress and the endothelium

Wall shear stress is sensed by endothelial cells via multiple wall shear stress-responsive cell components, which (de)activate intra-cellular pathways leading to regulation of gene and protein expression. This force-induced regulatory process plays a continuous role in the development, growth, remodelling, and maintenance of the vascular system (*Table 1* and *Figure 2*). Generally, endothelial cells exposed to high, unidirectional wall shear stress assume a quiescent state, while endothelial cells exposed to low and/or directional varying wall shear stress are activated, displaying a pro-inflammatory state.[4] There is also an important interplay between wall shear stress and pro-inflammatory cytokines such as tumour necrosis factor (TNF) and interleukin (IL)-1β. These cytokines function as central drivers of arterial inflammation by inducing endothelial expression of adhesion protein and chemokines that co-operate to capture leukocytes from the blood stream to the vessel wall. High shear stress reduces the ability of TNF or IL-1β to activate EC whereas low shear stress primes them for pro-inflammatory responsiveness.[5–8] Recently, the Canakinumab Anti-inflammatory Thrombosis Outcomes Study (CANTOS) revealed that targeting of IL-1β led to reduced cardiovascular events in patients with a previous myocardial infarction, thereby highlighted the importance of IL-1β in atheroprogression.[9] The molecular mechanisms underlying the pro- or anti-inflammatory effects of wall shear stress are governed by wall shear stress-responsive transcription factors. The anti-inflammatory transcription factors KLF2 and Nrf2 are activated by high wall shear stress and have been shown to be involved in the regulation of 70% of high wall shear stress-induced genes. In contrast, the transcription factors AP-1 and NF-κB are activated by low and/or oscillatory wall shear stress and positively regulate pro-inflammatory genes.[10–15] The wall shear stress responsive pathways also regulate endothelial function and vessel integrity. This includes short-term regulation of vascular tone, via release of potent vasodilators (e.g. nitric oxide) and vasoconstrictors (e.g. endothelin-1), respectively, but also long-term processes including vascular remodelling (e.g. outward/inward remodelling, angiogenesis, and collateral formation) to meet tissue perfusion demand. This section provides a brief overview of some of the most important mechanisms and pathways that relate wall shear stress to atherosclerosis and restenosis. For a more detailed description of these and other pathways, and their role in priming of endothelial cells, the reader is referred to other review articles.[16,17]

Table 1 Levels of shear stress and its effects on atherosclerosis

Label	Range (Pa)[18–22]	Effects in: Early atherosclerosis[4]	Advanced atherosclerosis[4]	Stented segments[23,24]
Oscillatory	0 ± 0.5	Athero-prone	Athero-prone	Neoathero-prone
Low	0–1			
Normal/high	1–7	Athero-protective	No consensus[a]	Neoathero-protective
Elevated	>7	NA	Erosion	NA

In cultured endothelium, 0 ± 0.5 Pa is often used to mimic athero-prone shear stress, whereas 1.2–1.5 Pa is the most frequently used value to simulate normal, often termed high, arterial shear stress. Consistent with this, a low, oscillatory shear stress of 0.05 ± 0.5 Pa was measured in the disease prone region of the internal carotid artery[18,19] and in healthy human coronary arteries, time-averaged wall shear stress was found to be approximately 1.4 Pa.[20] In atherosclerotic human arteries, shear stress can vary with changes in geometry. It is elevated at the stenosis of plaques reaching >7 Pa in some instances.[21] In cultured endothelium, 7.5 Pa is used to mimic elevated shear stress *in vitro*.[22] However, it should be noted that low shear stress is associated with plaque progression in diseased human coronary arteries.[25] The effect of shear stress profiles on early and late atherosclerosis are reviewed in reference 4, and their effect on neoatherosclerosis in stented vessels are reviewed in references 23 and 24.
NA, not applicable.
[a]See Supplementary material online, *Appendix B, Table B1*.

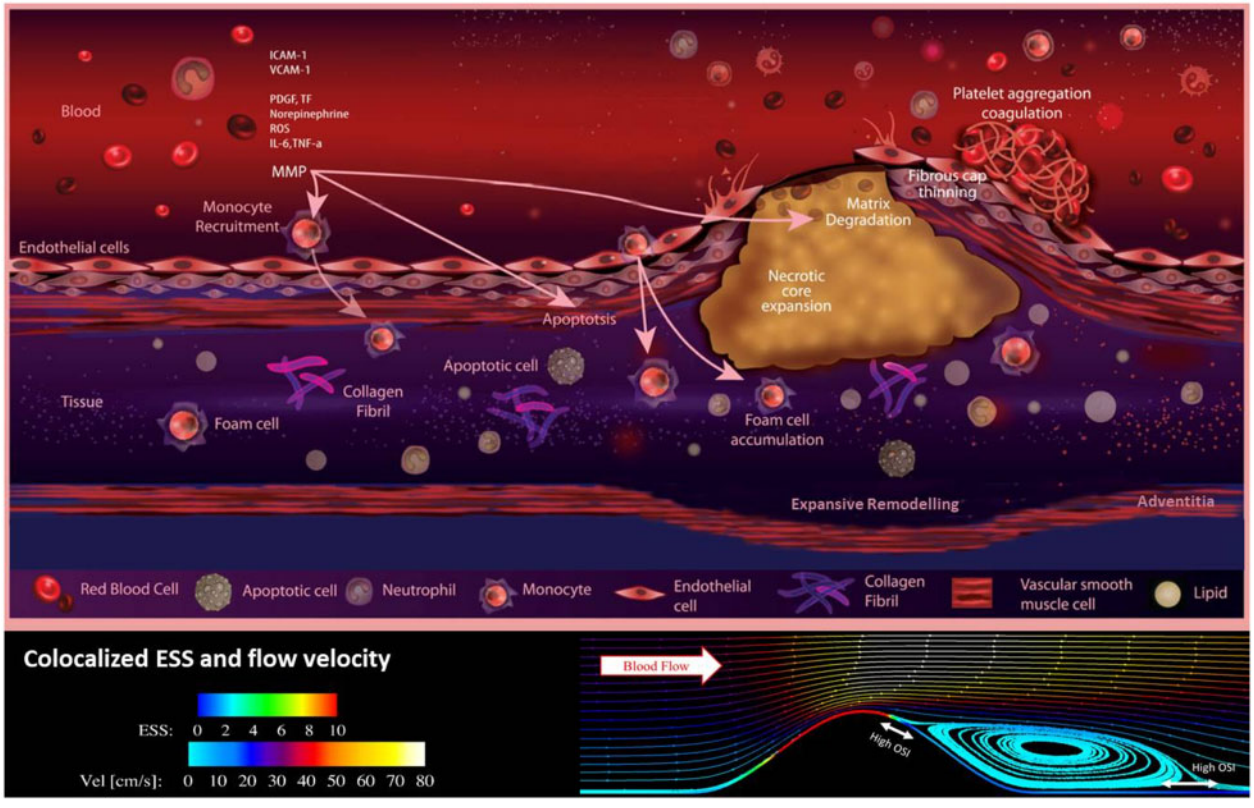

Figure 2 A schematic illustration of some of the processes that are involved in plaque development and rupture, and how these are related to wall shear stress. In low wall shear stress regions, monocytes are recruited by the endothelium through the expression of various adhesion molecules. Recruited monocytes transform into foam cells which subsequently can accumulate and are the main source for the development of the necrotic core. Expansive remodelling initially prevents lumen intrusion of the plaque, but once this process fails, the wall shear patterns the plaque is exposed to changes. High wall shear stress will be present at the upstream part and the throat of the plaque, while in the downstream region, low wall shear stress will be accompanied by elevated levels of oscillatory flow. Although there is no direct effect of wall shear stress on plaque rupture, shear stress does influence endothelial function, potentially leading to cap thinning in the high wall shear stress regions.

Wall shear stress and early atherosclerosis

Many of the same signalling pathways that regulate developmental, homeostatic, and adaptive mechanisms in arteries play a key role in the development of coronary artery disease initiation and progression, partly explaining site specific susceptibility to atherosclerosis.[26] The low and/or oscillatory wall shear stress-induced inflammatory activation of the endothelium typically occurs at the inner bend of curved arteries, ostia of branches, lateral walls of bifurcations, at surgical junctions such as end-to-side anastomoses, and up or downstream from luminal obstructions. At these sites, circulating inflammatory cells, primarily monocytes, interact with adhesion molecules like vascular cell adhesion molecule (VCAM)-1 and monocyte chemotactic protein (MCP)-1 (transcriptional targets of AP-1 and NF-κB), expressed on the activated endothelial cells. The monocytes then enter the sub-endothelial layer where they become macrophages that engulf lipoproteins and subsequently transdifferentiate into foam cells, trapping them inside the arterial wall and leading to atherosclerotic plaque initiation: the fatty streak. During progression of atherosclerosis, the plaque grows. Initially the artery will remodel outward to preserve lumen area and tissue perfusion, thereby maintaining the wall shear stress profile before lesion onset and promoting the pro-inflammatory activation of the endothelium now overlying the plaque. In this way, low wall shear stress continues to contribute to early plaque growth. In contrast to branches and bifurcations, regions of arteries with uniform geometry are generally exposed to laminar flow and undisturbed wall shear stress which induces anti-inflammatory and athero-protective processes, in part, via activation of KLF2 and Nrf2 which suppress inflammatory and pro-apoptotic signalling pathways.[11]

Wall shear stress and advanced atherosclerosis

In the advanced stages of the disease, both high and low wall shear stresses have been suggested to play a detrimental role. Plaques vary in terms of geometry and composition. Some have a preserved lumen that is continuously exposed to their original wall shear stress, either low in curved segments or oscillating in bifurcations, while others have a narrowed lumen that is mainly exposed to increased spatial and temporal variations in wall shear stress.[26] In both cases, wall shear stress may influence plaque composition, leading to varied risk of plaque vulnerability. In coronary plaques with a preserved lumen, low wall shear stress has been correlated to a reduction in smooth muscle cells, reduced collagen production, and increased metaloproteinase activity.[27]

Two-thirds of acute coronary syndromes are caused by plaque rupture. One-third demonstrates a thrombus overlying a non-ruptured plaque, in which the event appears to be caused by endothelial erosion.[28] Less is known about the mechanisms regulating plaque erosion than those for plaque rupture. It has been suggested that both high and low wall shear stress can be causative of erosion.[29,30] Unlike plaque rupture, endothelial erosion tends to occur on stable, thick-capped atherosclerotic plaques.[31] On these stable, inward remodelled plaques, endothelial apoptosis, and loss of endothelial contact with the underlying extracellular matrix are processes believed to be involved in endothelial erosion and have been shown to be induced by high wall shear stress (reviewed in reference[31]) However, endothelial detachment was observed to be twice as frequent on the downstream side of lumen narrowing plaques,[32] suggesting a role for low and/or oscillatory wall shear stress.[33] These apparently conflicting observations suggest that biological mechanism, in concert to wall shear stress, may play a role in this process.

Wall shear stress and in-stent restenosis

It has been proposed that wall shear stress also plays an important role in stented arteries.[34] Stents alter local artery geometry and concomitantly wall shear stress patterns. If the deployed stent is patent and without luminal irregularities, the local wall shear stress pattern will be primarily physiologic or vasculoprotective. If the artery geometry is curved or tortuous, however, then by restoring the three-dimensional (3D) geometry present before lumen intrusion, the wall shear stress profile that caused the disease may be reinstated. In addition, the presence of stent struts, depending on their height and width, can lead to the generation of disturbed wall shear stress in between the struts.[35–38] Furthermore, stent implantation may increase the local curvature at the entrance and exit of the stent, further enhancing disturbed shear stress regions.[23] Higher wall shear stress on the adluminal surface of the struts induces platelet activation and modifies their morphology.[39] The activated platelets resume their discoid geometry as they enter the lower wall shear stress zones within the recirculation zone behind the struts, causing conformational changes in von Willebrand receptors and platelet aggregation.[40,41] Furthermore, low, disturbed wall shear stress zones beside the struts can induce the platelets to release platelet-derived growth factor that stimulates endothelial proliferation in these stagnation zones.[42,43] The higher wall shear stress on top of the struts results in poor endothelialization,[44] while the low, disturbed wall shear stress in the vicinity of the struts reduces endothelial migration[38] and initiates smooth muscle cell migration into the subintimal layer.[45] Through all these mechanism presented above, wall shear stress has been associated with neointima development and neoatherosclerosis (neoatherosclerosis biological mechanisms are reviewed in references 23 and 38) in human coronary arteries which can ultimately result in the need for repeat interventions.[38]

Imaging coronary arteries: a brief review

Why is three-dimensional luminal data so important?

Assessment of haemodynamic parameters requires a precise imaging and 3D reconstruction of the lumen geometry. In general, coronary arteries are imaged using traditional X-ray angiography, multi-slice computed tomography angiography (CTCA), magnetic resonance imaging, and various intravascular imaging techniques including intravascular ultrasound (IVUS), optical coherence tomography (OCT), and near-infrared spectroscopy (NIRS)-IVUS. In addition, several other invasive imaging modalities are under development and may have future applications in coronary reconstruction and overcome limitations of the existing techniques enabling detailed assessment of plaque morphology.[46]

Geometry assessment with invasive and non-invasive coronary angiography

With traditional X-ray angiography, the contrast filled lumen of the coronary arteries is visualized using X-rays, generating a 2D projection of the arterial lumen, with a pixel size of 150–250 μm. Combining information from two or more X-ray images selected at the same moment during the cardiac cycle, a 3D reconstruction of the coronary artery lumen can be generated.[47–50] Due to their ease of application, and the widespread availability of angiography, these 3D reconstruction techniques have been incorporated in commercially available software.[51] However, the accuracy of coronary angiography-based wall shear stress computations remains controversial, as some studies have demonstrated a moderate association between the wall shear stress estimated in angiographic-based models and those reconstructed from intravascular imaging, while others have shown a strong correlation.[52–55] On the other hand, there is robust evidence on its efficacy in calculating haemodynamic parameters which are less sensitive to the exact lumen shape, such as FFR, which is defined as the ratio of pressure distal to the lesion to the proximal pressure.[56] The efficacy of CFD analysis in models reconstructed from multiple angiographic projections or rotational angiography in predicting the FFR has been validated against *in vivo* measurements with promising initial results.[57–60]

Computed tomography angiography enables reconstruction of the entire coronary tree and it can be used to study plaque distribution in coronary bifurcations and the effect of the local haemodynamic forces in these vulnerable segments.[61] These advantages however come at a cost of a lower imaging resolution (240–500 μm) and less reliable characterization of the composition of the plaque; limitations that are likely to have an impact on the estimated wall shear stress and affect the association between local haemodynamic forces and plaque characteristics.[62,63] Several recent studies however, have used CTCA-based models to evaluate wall shear stress[64] and two reports have shown that computational modelling in CTCA-based reconstruction can provide useful information and predict segments that will exhibit atherosclerotic disease progression highlighting its value in the study of atherosclerosis.[65–66]

Magnetic resonance imaging has also been utilized to reconstruct 3D anatomical models for CFD analyses but its image resolution is limited for coronary arteries (resolution 1000–1340 μm); therefore this modality is currently not recommended for coronary artery lumen reconstruction.

Imaging approaches based on fusion with intravascular techniques

To overcome the limitations of angiography and CTCA, and to reconstruct high-resolution models of the coronary arteries fusion of angiography or CTCA and intravascular imaging has been proposed.[67–72] These methods benefit from the high spatial resolution of the non-X-ray based imaging modalities in each cross-section and allows imaging of the vessel wall and its components.[73–75] Coronary reconstruction based on fusion of IVUS or OCT and angiography or CTCA includes the following steps: (i) the extraction of the IVUS catheter path or the lumen centreline from two end-diastolic angiographic projections, (ii) the segmentation of the end-diastolic IVUS or OCT frames, (iii) the placement of the contours perpendicularly onto the catheter path or the lumen centreline and the estimation of their relative twist using the Frenet–Serret formula or the sequential triangulation algorithm, and (iv) the comparison of the silhouette of the back-projected lumen model with the lumen silhouette on the angiographic projections[67,68] *or* the use of anatomical landmarks visible in both IVUS or OCT and X-ray imaging or CTCA[69–71] to estimate the absolute orientation of the IVUS or OCT frames (*Figure 3*).[71]

Intravascular ultrasound was the first invasive imaging modality that was used to reconstruct coronary anatomy. This modality with its high penetration depth enables assessment of luminal morphology and plaque burden and has provided unique insights about the role of wall shear stress on atherosclerotic evolution.[26,73] A limitation of IVUS is its limited efficacy to assess plaque composition and its low resolution (65–150 μm) that do not allow microscopic evaluation of plaque pathology. Near-infrared spectroscopy-intravascular ultrasound imaging appears able to assess more accurately plaque tissue characteristics and today synergistic ability to identify plaque components has been shown.[76]

Another modality that enables accurate evaluation of the superficial plaque is high-resolution OCT (12–18 μm) that is able to assess plaque micro-characteristics associated with plaque vulnerability that are unseen by IVUS such as the fibrous cap thickness, neovessels, cholesterol crystals, and macrophages accumulation.[77] Moreover, OCT, in contrast to IVUS, allows visualization of the lumen protruded struts in stented and scaffolded segments that, as it has been shown in *in silico* studies, can create micro flow disturbances and recirculation zones in the areas between the struts.[23,78] Therefore, OCT-based 3D reconstruction of stented segments is currently considered superior to IVUS-based strategies,[79] and the available strategies are discussed in more detail in 'Geometrical model construction and meshing procedure' section.

Preferred imaging modality for assessing wall shear stress in different clinical scenarios

- Studies aiming to investigate the effect of wall shear stress on plaque progression and changes in plaque composition should preferably create coronary artery models using fusion of IVUS/NIRS-IVUS and coronary angiography or CTCA.
- Studies aiming to investigate the influence of the local wall shear stress on plaque micro-characteristics should preferably create the 3D lumen using fusion of OCT and biplane angiography or CTCA.
- Studies aiming to investigate the influence of the local wall shear stress distribution in a stented regions should preferably create the 3D lumen using fusion of OCT and biplane angiography or CTCA.
- 3D quantitative coronary angiography (QCA) and CTCA have limited accuracy in evaluating lumen and vessel wall anatomy but it can be considered to assess the wall shear stress and FFR on plaque evolution in low-risk patients where intravascular imaging is not an option.
- Magnetic resonance imaging-based lumen reconstructions are currently not accurate enough for assessment of the wall shear stress distribution.

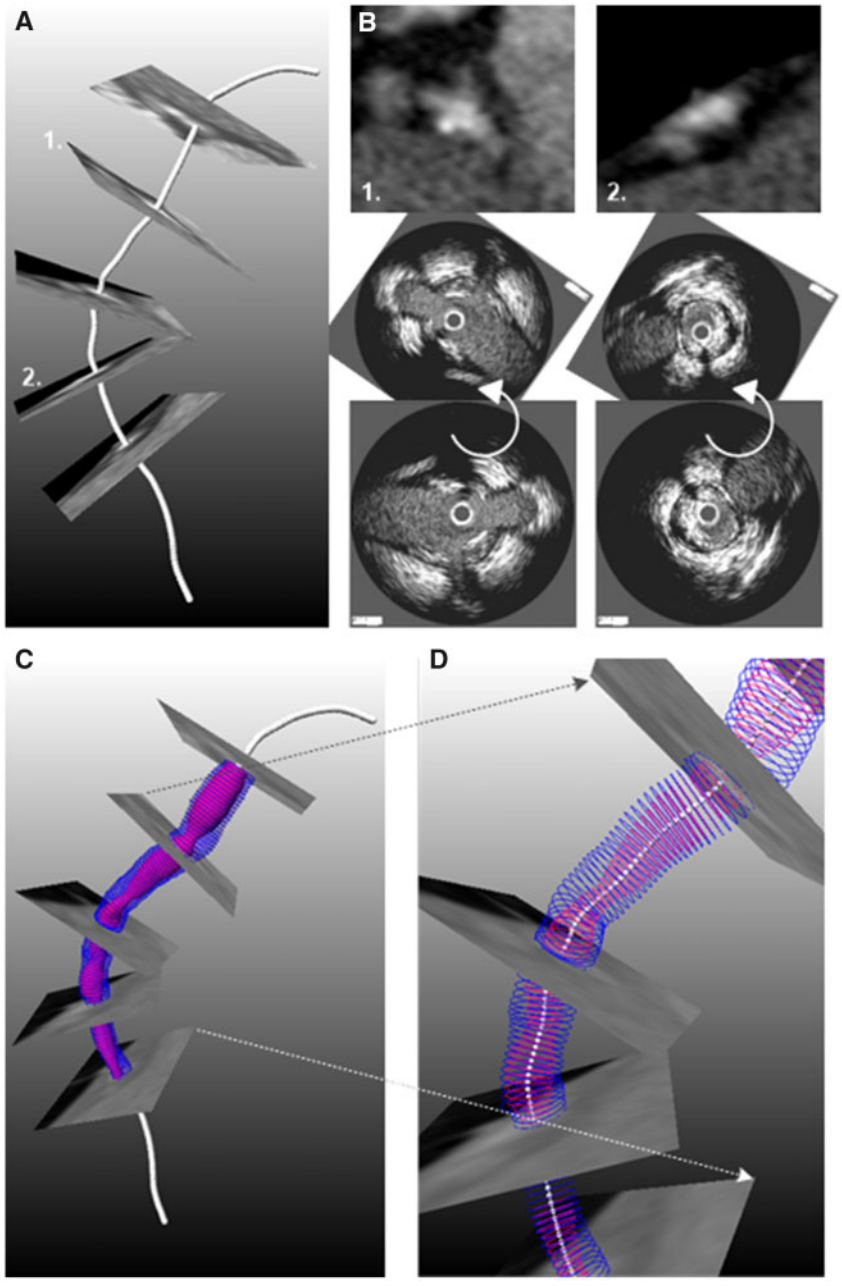

Figure 3 Methodology developed to fuse computed tomography angiography and intravascular imaging data:[71] (*A*) Extraction of lumen centreline from computed tomography angiography. (*B*) Cross-sectional computed tomography angiography images are generated perpendicularly to the centreline and anatomical landmarks that are seen in intravascular ultrasound/optical coherence tomography images are detected. After matching the intravascular imaging contours are rotated so as to obtain the correct orientation (middle panel). (*C*) The orientated intravascular imaging contours are placed perpendicular to the lumen centreline extracted by computed tomography angiography to reconstruct the coronary artery anatomy that is shown in (*D*).

Wall shear stress in native arteries

Wall shear stress inside the coronary artery lumen can be simulated by numerically solving the mathematical equations governing the motion of the arteries and blood flow with relevant boundary conditions.[80] The system as a whole represents a complex fluid–solid interaction (FSI) problem. However, it was demonstrated that full FSI analysis (i.e. including the motion of the walls of the heart) of the right coronary artery only accounts for ~5% difference in the most widely

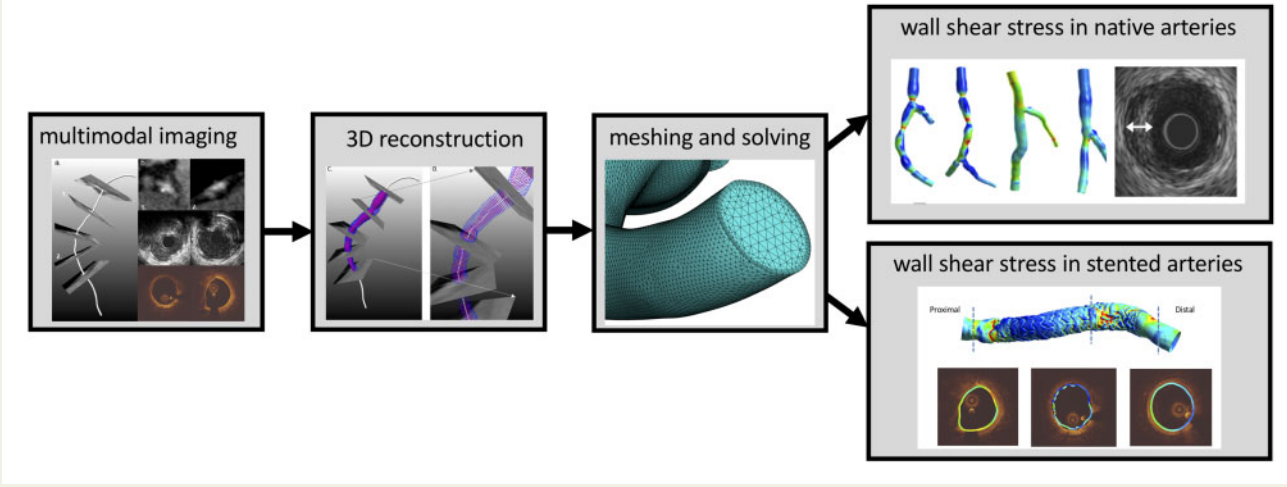

Take home figure Wall shear stress in coronary arteries from imaging to modelling.

used metric, the time-averaged wall shear stress in a recent study.[81] For detailed information, the reader is referred to reference 82. In this section, we will focus on wall shear stress computations in coronary arteries with rigid, non-deforming walls. Recommendations will be provided for 3D geometry reconstruction of the artery lumen; the boundary conditions and material properties of blood needed to conduct the CFD simulations, the available software platforms (CFD solvers), and post-processing techniques for wall shear stress analysis (*Take home figure*). Technical details for Wall shear stress in native arteries and Wall shear stress in stents sections are provided in Supplementary material online, *Appendix A*.

Geometrical model construction

The characteristics of blood flow in the coronary arteries are strongly dependent on the 3D curvature, the presence of bifurcations, and lumen intruding plaques as well as the pulsatile nature of the flow (*Figure 4*). These geometrical and physical parameters will introduce haemodynamic features such as secondary flow and/or recirculation,[83] which will play a critical role in determining the wall shear stress dynamics at the region of interest (ROI). The inclusion of the proximal segment of the coronary arteries allows for a natural development of the secondary flow, which is essential for an accurate representation of the distal wall shear stress pattern.[84] Therefore, segmentation and 3D reconstructions, whether it is from CTCA, 3D-QCA, IVUS, or OCT,[85–88] should be extended to the ostium of both right and left coronary artery whenever possible.

In addition, the presence of arterial bifurcations has a major impact on wall shear stress patterns.[89] Firstly, there is a global effect of bifurcations on wall shear stress. At each bifurcation, coronary flow is distributed between the main vessel and side branch, mainly depending on their diameters.[90,91] This leads to a reduction of blood flow in the main vessel, which is typically accompanied by tapering of the lumen of the mother vessel. Secondly, coronary bifurcations also have a local effect of wall shear stress patterns, inducing local regions of disturbed flow, potentially containing reversal of flow due to the presence of macro-recirculation (*Figure 4C*). Selection criteria to determine what side branch should be included can be found in Supplementary material online, *Appendix A.1*.

Meshing procedure

The reconstructed 3D geometries will be filled with grid points which represent the volume of the blood within the ROI. These grid points form the basis for the mesh elements, which are required to compute velocity and pressure from the governing equations for blood flow. In this meshing procedure, the individual grid spacing, or mesh size, is determined by the complexity of the arteries of interest. Generally, a finer grid spacing is required in the regions where large changes in the velocity profiles (see also *Figure 1*) are anticipated. This implies that a smaller elements are often used at the vessel wall, while larger elements are admissible in the central part of the artery, where the smaller changes in the velocity profiles are present (see also Supplementary material online, *Appendix A, Figure A2*). The optimal grid spacing needs to be determined by a mesh convergence analysis to demonstrate that further mesh refinement will not result in significant changes to the wall shear stress estimations. This is an essential step for each CFD analysis (see also Supplementary material online, *Appendix A.3*).

Boundary conditions

For CFD in coronary arteries in a rigid geometry, boundary conditions need to be described for the inlet, the outlet(s), and the arterial wall.

In steady flow simulations, the inflow velocity used is a time-averaged value over a cardiac cycle and time variation of the velocity at the inlet is neglected. The value for the time-averaged inlet can be obtained using either thrombolysis in myocardial infarction (TIMI) frame count,[90] including a modified TIMI frame count through the calculated true 3D reconstructed volume of the lumen segment of interest,[92] or a more sophisticated—but less widely available—intracoronary Doppler ultrasound blood flow velocity measurement.[93] If patient-specified flow measurements are not available, scaling laws can be applied. Various scaling laws are available that relate the local

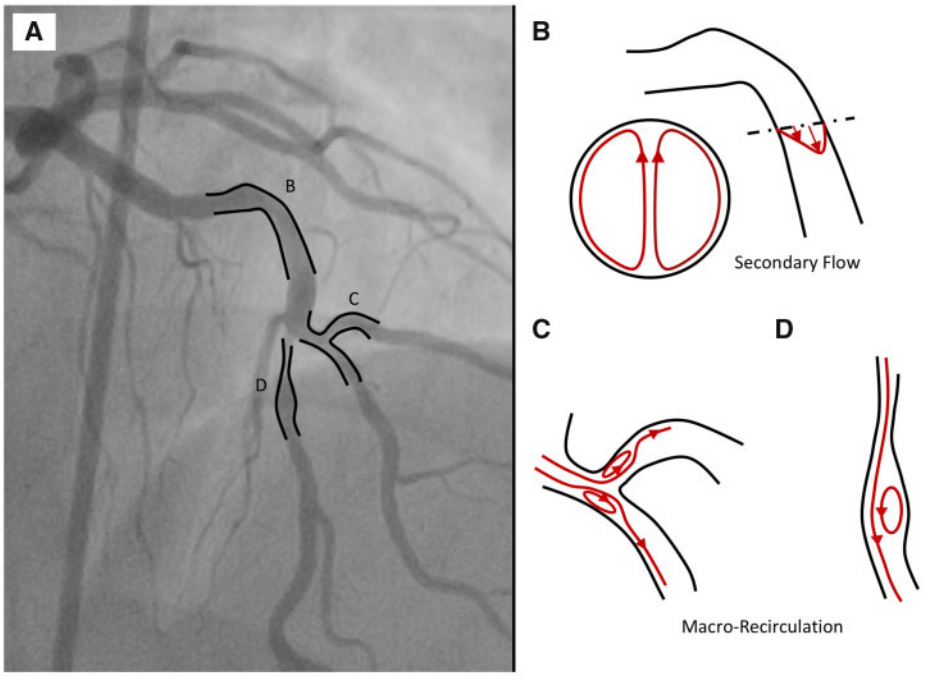

Figure 4 (*A*) Coronary tree showing multiple curvatures and bifurcation. (*B*) Secondary flow in the presence of the proximal curvature. (*C*) Macro-recirculation due to varying lumen geometries such as bifurcation and stenosis.

diameter of the artery to the average velocity.[94–96] In a coronary artery bifurcation study, the redistribution of coronary flow between the main vessel and side branch should be considered carefully. Ideally, patient-specific data should be used to determine the flow redistribution. These data can be obtained during clinical procedures, e.g. based on computed tomography perfusion[97] or myocardial volume.[91] If these are not available, one can use a diameter based scaling laws.[98,99] A constant pressure boundary at the model outlets can be applied to regulate the flow redistribution. Lastly, a no-slip and no-penetration boundary condition is prescribed at the arterial wall.

In recent years, interest in faithfully recreating the pulsating coronary fluid environments has become more common due to the additional information that can be obtained from analysing the temporal variation of wall shear stress.[83,100] The pulsatile nature of coronary flow can only be fully revealed with transient or unsteady CFD simulations. Suitable modifications to the boundary conditions at both inlet and outlet are needed to capture the coronary flow phasic behaviour (Supplementary material online, *Appendix A.4*). In particular, the difference between phasic coronary flow in the left and right coronaries should be accounted for. With velocity-derived inlet boundary condition, the time-varying inflow velocity can be derived from patient-specific measurements,[92,93] or the time-averaged velocity values can be combined with a generic velocity waveform.[90,101,102] At the outlet, the implementation of specialized coronary boundary condition model is needed if the phasic change in coronary pressure in pulsatile CFD analyses are studied.[103,104] Another commonly used boundary condition method is to couple the inlets and outlets to lumped parameter circuit models representing cardiac and coronary physiology via an analogy to electrical circuits and is described in details in Supplementary material online, *Appendix A.4*.

Blood rheology

Blood comprises a mixture of red blood cells (RBC), white blood cells, platelet, and plasma. Herein, we focus on one of the predominant features of blood, namely the ability of RBC to aggregate and elongate under different flow conditions, and the resulting effect on blood viscosity and subsequent impact on the wall shear stress calculation. It has been shown that at low shear rate,[105] RBCs aggregate and eventually form 'rouleaux' which in turns increases the viscosity of the blood (*Figure 5*).[106] However, RBC aggregation is a reversible process. That is, rouleaux begin to break up with increasing shear rate and return to single individual RBCs. The separation of RBCs from rouleaux results in an initial decrease in local blood viscosity that ultimately asymptotes to a constant value at higher shear rate.[107] This fluid behaviour of viscosity being inversely proportional to the shear rate is often referred to as a shear-thinning behaviour, making blood a non-Newtonian fluid. Most CFD simulations have simplified the shear-thinning fluid behaviour of blood to a Newtonian fluid using a constant blood viscosity of 3.5–4.0 mPa·s.[108] However, it is advised to implement suitable shear-thinning model (e.g. Carreau–Yasuda model[109] and Quemada model[110]) in coronary flow CFD studies.

Solution strategies

The solution procedure in CFD simulations involves various steps, each with their own settings that determine the solution accuracy. These settings are extremely important and depend on many factors,

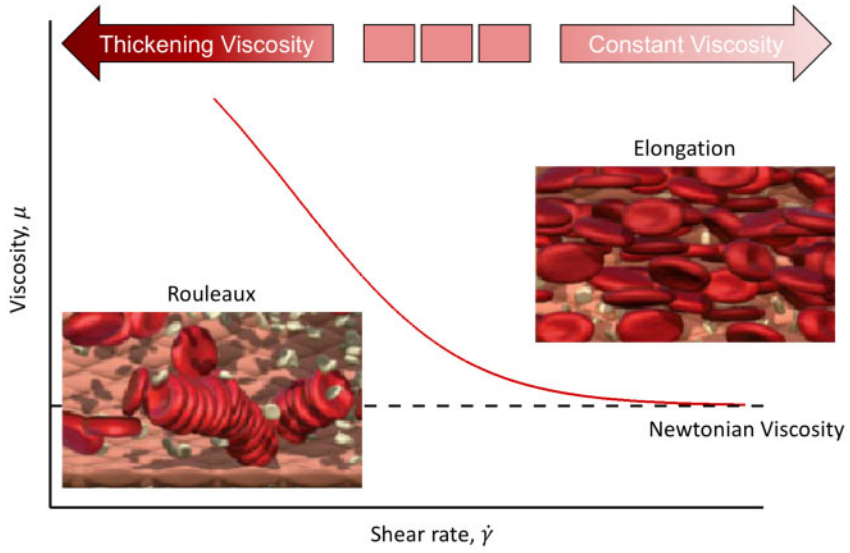

Figure 5 Changes in red blood cells under shear. Red blood cells aggregate at low shear rate, resulting in high blood viscosity. The process is reversed as shear rate increases.[106]

Table 2 Commonly used computational fluid dynamic software platforms

	Commercial/ open source	Remarks
ANSYS fluent STAR-CMM+ COMSOL	Commercial	Excellent user-interfaces and more technical support, but offer less control over the process
OpenFoam SimVascular Crimson	Open source	Require a high level of expertise to ensure appropriate implementation, but provide the necessary tools to customize the computational procedure.[a]

[a]SimVascular[113] provides various plug-ins that allow implementation of appropriate lumped parameter models, and tutorials on how to run coronary simulations.

including the solution method used, and on the flow regime. The appropriate choice of these settings requires engineering skills and in-depth knowledge about computational methods.[111,112] A key concept in the solution procedure is convergence. In CFD simulations, the Navier–Stokes equations are solved in an iterative manner. For each iteration, the error in solving the equations should reduce and the solution is said to be 'converged' when residual (error) values of velocity and pressure are below a certain threshold (see also Supplementary material online, *Appendix A.5*). Only converged solutions provide reliable wall shear stress maps. A list of CFD software platforms that are available and used in the community is provided in *Table 2*.

Post-processing

Several metrics can be derived from the computed wall shear stress distribution. Wall shear stress values up to about one to two vessel diameters after the inlet and about half or one vessel diameter length before the outlet side of geometry may have artificial values related to the boundary conditions and should be excluded from analyses. Wall shear stress metrics including temporal components include the oscillatory shear index,[18] relative residence time,[114] and a recently introduced metric called the transverse wall shear stress.[115] For a visualization of these quantities, the reader is referred to Supplementary material online, *Appendix A, Figure A4*.

Statistical analysis of the above quantities often requires mapping (in both circumferential and axial directions) of the CFD results to the cross-section contours in the ROI. It is important to emphasize that both mapping should be performed based on the resolution of the mesh, and the resolution of the medical imaging data, especially in case of IVUS and OCT-based CFD analyses. Further recommendations can be found in Supplementary material online, *Appendix A.6*.

Main recommendations for 'wall shear stress in native arteries'

- Arterial lumen reconstructions from ostium of both right and left coronary artery proximal to ROI need to be included for physiological blood flow development.
- Bifurcation reconstructions, especially immediately proximal to the ROI, are essential for accurate computation of the local wall shear stress distributions.
- The arterial lumen containing the blood is represented by thousands or even millions of mesh elements and the appropriate element size can only be determined by a mesh refinement study.
- Simulation results with 3% discrepancy or less at each mesh refinement step are considered mesh independent.
- Non-Newtonian blood properties should be accounted for by implementing suitable shear-thinning model.
- Each CFD simulation should be carefully checked on convergence, and convergence criteria depend on the problem at hand and the solution strategy.

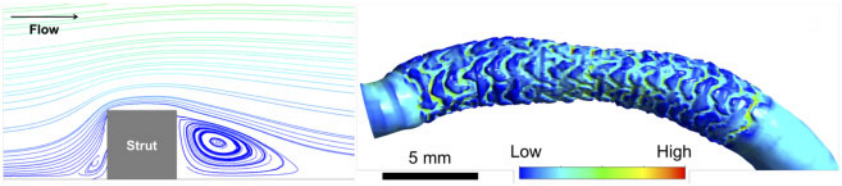

Figure 6 Overview of micro flow environment around a stent strut (left) and the resulting high and low wall shear stress regions around the strut (right).

- Wall shear stress and its variants are related to various pathological processes, and appropriate processing of the data depends on what process is studied.

Wall shear stress in stents

Simulation of blood flow in stented arteries adds another layer of complexity compared to flows in native arteries—flow around the stent struts creates small vortices on the order of the size of struts (*Figure 6*). Such small-scale flow characteristics can be labelled as the micro-environment whereas the flow patterns in the scale of the whole vessel, primarily determined by vessel curvature and narrowing, can be called the macro-environment. The flow around a strut is characterized as a region with accelerated flow, causing high wall shear stress on the abluminal strut surface and a recirculation zone at the downstream side of the strut, depending on the flow speed and strut shape. Due to the small size of the stent struts, and the flow features associated with them, special care needs to be paid when performing CFD in stented segments.

Geometrical model construction and meshing procedure

Reconstruction of a stented artery is challenging and requires reconstruction of the vessel lumen with struts protruding inward, as if the pattern of strut is imprinted on the native vessel border (*Figure 6*). The geometry reconstruction is even more complex when the strut is mal-apposed since there are small gaps between the struts and the vessel wall.

In order to capture the flow features around a strut, a very high mesh resolution is required (see Supplementary material online, *Appendix A.2* for technical details). At the same time, use of a 2D approximation and/or localized model around a strut (or a series of struts) is still an option depending on the research question such as comparison of hypothetical stent implantation scenarios using different strategies.[36]

Blood rheology

Blood properties may require an additional consideration when dealing with micro flow environment as the size of RBCs (6–8 μm) are roughly in the same order of magnitude as the struts (tens of μm), which can potentially affect flow patterns. Around the top of the strut, the difference between Newtonian approximation and non-Newtonian model may not be substantial because shear rates are high.[116] On the contrary, shear rate in the flow recirculation behind the strut is low and the impact of the blood viscosity model in determining the patterns of the flow is expected to be higher. Blood particles can be considered in a multiscale approach by allowing them to aggregate, forming rouleaux, and interact with flow. The importance of including blood particles in flow simulations on this scale is an open question: the presence of a cell-free layer near the arterial wall is well documented[117] in small arteries and arterioles but not adequately described in medium-sized arteries (diameter > 1 mm) like coronaries, especially with stents.

Solution strategy and post-processing

When blood is modelled as a homogenous fluid without particles, the solution procedure is generally the same as that for native arteries. However, additional attention is needed to the temporal resolution of the simulations (Supplementary material online, *Appendix A.5*). Additional models for the cellular volume and membrane for the blood cells are required in case these particles are accounted for. This is typically achieved by treating the volume occupied by RBCs as another fluid or phase with the cellular membrane as an interface.[118–120] Such models require much higher computing power and specialized solvers, particularly when the ROI is a whole vessel that should contain millions of RBCs. This type of computation in 3D has only been realized up to relatively short segment of vessels so far and supercomputers are typically required.[121,122]

Post-processing methods should be selected in accordance with the research question as outlined in Supplementary material online, *Appendix A.6*. When wall shear stress values are compared against plaque characteristics, the accuracy to co-register the two types of information needs to be considered to judge whether point-to-point comparison can be more reliable than comparison per segment. The amount of wall shear stress data from CFD is typically large, especially when comparing profiles changing over the time. Selecting an effective method to present the data such as the use of a histogram,[100,123] which can also be in a form of a cumulative curve, is important (Supplementary material online, *Appendix A, Figure A5*).

Main recommendations for 'wall shear stress in stents'

- Macroscopic flow patterns are determined by global vessel geometry, and microscopic flow pattern governed by stent struts. Both play important roles in determining wall shear stress distribution in stented vessels.
- High-resolution computational mesh generation is a key element to adequately capture the flow pattern, especially the micro-scale

features. Depending on the type of elements used, approximately ten elements are needed to discretize the height of a stent strut.
- The macroscopic effect of blood particles may be considered by incorporating non-Newtonian blood models. More physiologically realistic models of blood particles are needed to study the effect of individual particles, but such simulations still require unrealistically high computational demand.

Clinical applications

In vitro and *in vivo* animal studies demonstrate that wall shear stress is a potent modulator of endothelial function and influences the development of atherosclerosis.[124] As such, the major clinical interest in wall shear stress arises from its ability to identify patients at risk for future cardiovascular events or complications after stent placement. Many investigators have tackled this complex problem using various simulation techniques described above. Although several clinical CFD studies seem to reflect the observations of *in vitro* and animal experiments, findings in human patients are far from unanimous or clear-cut. This section summarizes clinical literature and steps that may be undertaken to propel CFD analysis into clinical application in the future. Supplementary material online, *Appendix B* contains tables that synopsize the clinical studies in native arteries (Supplementary material online, *Table B1*) and stented arteries (Supplementary material online, *Table B2*).

Wall shear stress in human native coronaries

A large body of studies has investigated wall shear stress in relation to coronary plaque morphology in native coronary arteries. Intravascular ultrasound-based CFD studies have associated low wall shear stress with enlargement of plaque area and necrotic core,[73,125] increased plaque eccentricity,[126] and reduction in lumen and vessel area.[25,127] Studies have also correlated high wall shear stress with progression of necrotic core and dense calcium in addition to regression of fibro-fatty and fibrous tissues.[73,128] The co-existence of high plaque burden both with low and high wall shear stress values improves prediction of plaque progression and vulnerability, respectively.[25,129] Optical coherence tomography-based CFD studies have similarly shown that low wall shear stress is correlated with a higher prevalence of lipid, with thinner fibrous caps[113,130] along with higher macrophage density and more superficial calcification.[130]

The largest trial examining wall shear stress in relation to clinical events was an IVUS-based analysis of 506 Japanese patients showing that low wall shear stress was able to predict lesions progressing to require percutaneous coronary intervention (PCI) during the 6–10 months of follow-up period.[25] Notably, however, most of these interventions ($n = 39/53$, 74%) occurred in asymptomatic patients treated for angiographic progression during protocol-mandated follow-up coronary imaging. Despite the relatively large number of patients studied, the number of symptomatic clinical events was too low to infer relationships with wall shear stress.

An alternative approach has been to retrospectively study patients with symptomatic clinical events. A recent *post hoc* CFD analysis of patients from the Providing Regional Observations to Study Predictors of Events in the Coronary Tree (PROSPECT) study compared baseline wall shear stress in patients with non-culprit plaques leading to major adverse cardiovascular events (MACE) with patients that did not develop MACE during 3.4 years of clinical follow-up.[131] The investigators demonstrated that the presence of low wall shear stress was significantly associated with the development of non-culprit MACE. In the presence of ≥2 anatomic risk factors such as high plaque burden, smaller minimal lumen area, or thin cap fibroatheroma morphology, lesions with low wall shear stress had a 3-year MACE rate of 52.1% compared to lesions with <2 anatomic risk factors and low wall shear stress (14.4%), vs. 0% in lesions with physiologic or high wall shear stress regardless of anatomic risk factors. These results suggest that low wall shear stress is important for clinically significant plaque progression, and that low wall shear stress incrementally improves the positive predictive value to identify patients at risk for future clinical events. However, the investigators were careful to point out that not all plaques with low wall shear stress developed MACE, and that it remains unclear which individual lesions will progress to cause clinical events.

The role of high wall shear stress is also gaining more interest in recent years. Intravascular ultrasound-based CFD studies of ruptured culprit plaques have demonstrated a strong correlation between focal elevation in wall shear stress and the site of plaque rupture.[132,133] An OCT-based CFD analysis of a single case demonstrated similar results.[134] Spatial co-localization cannot serve as evidence of causality; however, these studies suggest that identifying high wall shear stress over vulnerable atheroma may improve detection of plaques prior to rupture. A CTCA-based CFD study also showed that high wall shear stress had an incremental value over luminal narrowing in discriminating high-risk plaques.[64] The probability of high-risk plaques increased at both extremes of wall shear stress with the lowest at the physiological range of wall shear stress (≈40 dyne/cm^2). The Exploring the Mechanism of Plaque Rupture in Acute Coronary Syndrome Using Coronary CT Angiography and Computational Fluid Dynamics (EMERALD) study analysed 72 patients with clearly documented acute coronary syndrome (ACS) and available CTCA acquired between 1 month and 2 years before the development of ACS and showed that the non-invasive haemodynamic assessment including wall shear stress enhanced the identification of high-risk plaques that subsequently caused ACS. In that study, the average wall shear stress of 66 culprit lesions were significantly higher than that of 150 non-culprit lesions.[135] These findings were recently corroborated in a small cohort of the FAMEII trial, in which it was shown that high wall shear stress in the upstream part of a plaque contributed to the prognostic value of FFR to predict MI.[136]

Despite evidence correlating wall shear stress with atherosclerosis, advances on several fronts will be necessary if wall shear stress is to be used for identification of future culprit lesions. The most obvious and important one is the need for large, prospective, image-based clinical CFD studies evaluating hard clinical endpoints along with plaque morphology. However, since wall shear stress as it is currently determined does not contribute with sufficiently high sensitivity or specificity to accurately predict clinically significant progression of atherosclerotic plaques, additional methodological advances will also be necessary.

The use of high-resolution and multiple hybrid imaging modalities may provide additional information about how fluid dynamic measures relate to vascular pathophysiology. Improved imaging may also

aid arterial reconstructions through more detailed lumen/vessel geometry and facilitate the incorporation of side branches. In terms of CFD methodology, advances may include routine use of pulsatile flow conditions, non-Newtonian rheological models of blood, and complementary or novel fluid dynamic parameters. Naturally, ongoing improvements in computing power and streamlining of workflows are also expected to improve the online clinical application of these techniques.

Ultimately, with further advances it is anticipated that clinical CFD analyses will emerge as one of many diagnostic and prognostic tools in clinical practice. Regulatory bodies around the world have also increasingly acknowledged the importance of streamlining the approval process for new technologies, evidenced, for example, by the UK's Accelerated Access Review pathway. The development and approval of FFR_{CT} illustrates how wall shear stress analyses may similarly navigate the regulatory approval process as sufficient clinical data supporting their use emerges.

In terms of CFD simulation to calculate wall shear stress, another question remains how to use this data: clinicians must be prepared with the appropriate treatments. If future culprit lesions can be reliably identified, prospective treatment strategies theoretically include a combination of risk stratification, lifestyle management, systemic and/or targeted drug therapy, 'preventative' PCI, or any number of other interim developments. Work in this area is underway, but optimal strategies have yet to be defined. Given the small but non-trivial risk associated with PCI and stent/scaffold placement, pre-emptive interventional treatment has been difficult to justify thus far. However, prospective studies randomizing patients to various non-invasive pre-emptive treatments based on their CFD profile should be considered to identify the ideal treatment of future culprit lesions.

Main findings from clinical trials: wall shear stress in native arteries

- Both low and high wall shear stress have been associated with aspects of plaque progression and vulnerability by clinical imaging studies, but the precise relationships remain unclear and studies are sometimes contradictory.
- Low wall shear stress has been associated with future angiographically driven revascularization and non-culprit MACE.
- High wall shear stress has been associated with future myocardial infarctions.

Wall shear stress in stents

Treatment of coronary stenosis by PCI through the implantation of metallic or polymeric devices by definition induces flow alterations.[36] Patient, device, and procedural factors all play a role in the final macro- and micro-environmental flow profile.[137] The advent of patient-specific blood flow simulations has been instrumental in characterizing local haemodynamics of stented regions to better understand device healing and complications such as restenosis and thrombosis.[138]

At the macroenvironment, several geometric modifications occur after PCI that have a direct implication for the wall shear stress pattern. A step-up phenomenon in lumen area, frequently observed at the inflow of the treated region, alters the flow and has been associated with areas of low wall shear stress. In contrast, at the distal segment of the stented region a decrease in lumen area or step-down increases shear stress.[139] The clinical consequence of this kind of shear stress pattern has not been completely understood; however, several studies have linked low wall shear stress to neointimal hyperplasia formation after bare metal stent (BMS) implantation.[140] Low wall shear stress might trigger vascular smooth muscle migration, proliferation, and matrix formation which may lead to in-stent restenosis.[141]

Stent under-expansion has been shown to be associated with in-stent restenosis and thrombosis and also influence wall shear stress distribution,[24] with areas of high wall shear stress at the upstream and low wall shear stress at the downstream of the under-expanded region. Stent mal-apposition, another consequence of a sub-optimal implantation, was found to impact wall shear stress and arterial healing. Strut detachment from the vessel wall >100 μm induces flow disturbances affecting strut coverage at mid-term follow-up.[116]

At the microenvironment level, the interaction among stent struts, a denudated vessel wall and blood components may play a role as a substrate for stent thrombosis.[142] Refinements of the 3D reconstruction techniques for CFD simulations, using high-definition images from OCT made possible to investigate the impact of stent design and strut thickness *in vivo*. The wall shear stress distribution was found to fluctuate amongst the different region of the stent struts.[23,143] In front or at the inflow of the strut, areas of moderate to high wall shear stress have been described. At the top of the struts, high wall shear stress values have been correlated with shear-mediated activation of platelets and activation of von Willebrand factor.[144] Behind the struts, low wall shear stress with areas of recirculation promotes platelet aggregation which may predispose to thrombus formation and stent thrombosis in an endothelium activated by injury.[23,143] The magnitude of the blood flow alterations has been shown to be dependent on the height and thickness of the device struts.[142,145]

A sub-optimal wall shear stress immediately after stenting may serve for risk stratification based on CFD. It has been shown that, in wide range of follow-up period ($n = 36$, median 8.0 years, 0.4–16.7 years), the low wall shear stress immediately after stent implantation can be a predictor of neoatherosclerosis.[146] Here, the wall shear stress was quantified on vessel wall without reconstructing the actual stent strut structure and averaged wall shear stress over vessel wall segment was used in the analysis. This implies that wall shear stress on a smoothed lumen geometry after initial endotheliarization post-stent implantation can serve as a predictor, in cases of adequate stent expansion and strut apposition.

Several meta-analyses have demonstrated that first-generation metallic stents made from stainless steel and with thick-strut (>140 μm) are associated with worse clinical outcomes as compared to newer thinner strut drug-eluting stent (DES) (<100 μm).[147,148] Moreover, the advent of new-generation stents with reduced strut thickness has decreased the rates of in-stent restenosis and thrombosis.[148] Although, newer and thinner platforms exhibit enhanced haemodynamic profile and reduced blood flow alteration, the improvement in clinical outcomes cannot be attributed solely to the strut thickness but rather to a combination of improved polymer biocompatibility, new metallic alloys, and better stent design.

The field of CFD has allowed us to better understand the impact of coronary devices on blood flow disturbances and their consequences on arterial healing after PCI.[138] In the 2016 report, the Federal

and Drug Administration (FDA) recommended computational modelling of coronary stents as a tool to guide developments in the field.[149] The increasing amount of evidence correlating wall shear stress with arterial healing, neointimal formation, and thrombotic risk may translate CFD to clinical practice. The exponential growth of computer technology and expertise of bioengineers and clinicians have the potential not only to improve stent designs but also to guide stent deployment and ultimately PCI. Optical coherence tomography 3D lumen reconstruction after stenting with automatic evaluation of mal-apposition can be performed online. The combination with CFD for online wall shear stress assessment in stented regions to optimize stent deployment may be feasible in the near future. Nevertheless, clinical studies addressing the incremental value of the integration of CFD and wall shear stress are warranted. A number of clinical studies are ongoing to investigate the focal and potentially more global effects of adverse wall shear stress after stenting on device healing. These include the Shear Stent study (NCT02098876), Absorb III Imaging Sub-study (NCT01751906), and the ISR Flow study.

Main findings from clinical trials: wall shear stress in stents

- Neointimal thickness has been shown to be inversely correlated to wall shear stress.
- Low wall shear stress after BMS implantation was associated with neointimal hyperplasia formation. However, after DES low wall shear stress does not correlate with in-stent hyperplasia.
- After bioresorbable scaffold implantation, low wall shear stress promotes neointimal hyperplasia and contributes to scaffold healing with normalization of wall shear stress.
- There is an inverse association between baseline wall shear stress and the incidence of neoatherosclerosis in both BMS and DES.

Concluding remarks

Wall shear stress affects endothelial function, plaque progression, vascular remodelling, and arterial healing after PCI. Since wall shear stress cannot be measured directly in human coronary arteries, we solve the Navier–Stokes equations describing the motion of a fluid, using CFD. The results of CFD are greatly affected by the quality of the input data, especially the 3D geometrical data of the coronary artery lumen. In this article, we reviewed critically the proposed methodologies applied to obtain reproducible and reliable wall shear stress maps. Advances in methodologies integrating angiography or CTCA with intravascular imaging and improvements in computing power have enabled us to simulate wall shear stress in both native and stented coronary arteries. Currently, CFD is already applied in various clinical applications, mainly to compute pressure drop and determine FFR. The increasing amount of evidence correlating wall shear stress with e.g. neointimal formation and thrombosis can translate wall shear stress analyses into clinical practice. For example, we can evaluate the impact of the scaffold design, in particular of the strut thickness and shape and the alignment of strut connectors, on the local haemodynamic forces with these techniques. Apart from application in stented arteries, we also envision application of wall shear stress metrics in native arteries. One could for instance generate wall shear stress maps of all the coronary vessels, much like currently is done for FFR_{CT}, subdivide these maps into regions labelled according to the levels given in *Table 1*, and use these maps to predict location of plaque progression and plaque rupture. Although we acknowledge that additional clinical research is needed to identify the predictive strength of wall shear stress in atherosclerosis and stented segments, we expect that with further advances in imaging and computational power CFD analyses will be available as one of the major diagnostic and prognostic tools in routine clinical practice.

Supplementary material

Supplementary material is available at *European Heart Journal* online.

Conflict of interest: Dr C.C. reports grants from Bisensors, grants from HeartFlow, other from Phillips, grants from Abbott Vascular, outside the submitted work. Dr J.D. reports grants and personal fees from Acist Medical, grants and personal fees from PulseCath BV, grants and personal fees from Medtronic, grants from Boston Scientific, grants from Pie Medical, outside the submitted work. Dr E.E. reports grants from NIH R01 GM 49039 during the conduct of the study. Dr H.S. reports grants from Abbott Vascular, grants from Medtronic, grants from Pfizer, grants from Volcano Phillips, during the conduct of the study; personal fees from Volcano Phillips, personal fees from American College of Cardiology, outside the submitted work; In addition, Dr H.S. has a patent Provisional Patent Application # 18087 pending. Dr D.T. reports a patent Image-Based Computational Mechanical Analysis and Indexing for Cardiovascular Diseases issued. Dr J.W. reports grants from Erc starting grant agreement no. 310457 outside the submitted work.

References

1. Young DF, Tsai FY. Flow characteristics in models of arterial stenoses. I. Steady flow. *J Biomech* 1973;**6**:395–410.
2. Young DF, Tsai FY. Flow characteristics in models of arterial stenoses. II. Unsteady flow. *J Biomech* 1973;**6**:547–559.
3. Gould KL, Kelley KO, Bolson EL. Experimental validation of quantitative coronary arteriography for determining pressure-flow characteristics of coronary stenosis. *Circulation* 1982;**66**:930–937.
4. Kwak BR, Back M, Bochaton-Piallat ML, Caligiuri G, Daemen MJ, Davies PF, Hoefer IE, Holvoet P, Jo H, Krams R, Lehoux S, Monaco C, Steffens S, Virmani R, Weber C, Wentzel JJ, Evans PC. Biomechanical factors in atherosclerosis: mechanisms and clinical implications. *Eur Heart J* 2014;**35**:3013–3020; 3020a–3020d.
5. Passerini AG, Polacek DC, Shi C, Francesco NM, Manduchi E, Grant GR, Pritchard WF, Powell S, Chang GY, Stoeckert CJ, Davies PF. Coexisting proinflammatory and antioxidative endothelial transcription profiles in a disturbed flow region of the adult porcine aorta. *Proc Natl Acad Sci USA* 2004;**101**: 2482–2487.
6. Dai G, Kaazempur-Mofrad MR, Natarajan S, Zhang Y, Vaughn S, Blackman BR, Kamm RD, Garcia-Cardena G, Gimbrone MA Jr. Distinct endothelial phenotypes evoked by arterial waveforms derived from atherosclerosis-susceptible and -resistant regions of human vasculature. *Proc Natl Acad Sci USA* 2004;**101**: 14871–14876.
7. Chiu JJ, Lee PL, Chen CN, Lee CI, Chang SF, Chen LJ, Lien SC, Ko YC, Usami S, Chien S. Shear stress increases ICAM-1 and decreases VCAM-1 and E-selectin expressions induced by tumor necrosis factor-alpha in endothelial cells. *Arterioscler Thromb Vasc Biol* 2004;**24**:73–79.
8. Partridge J, Carlsen H, Enesa K, Chaudhury H, Zakkar M, Luong L, Kinderlerer A, Johns M, Blomhoff R, Mason JC, Haskard DO, Evans PC. Laminar shear stress acts as a switch to regulate divergent functions of NF-kappa B in endothelial cells. *FASEB J* 2007;**21**:3553–3561.
9. Ridker PM, Everett BM, Thuren T, MacFadyen JG, Chang WH, Ballantyne C, Fonseca F, Nicolau J, Koenig W, Anker SD, Kastelein JJP, Cornel JH, Pais P, Pella D, Genest J, Cifkova R, Lorenzatti A, Forster T, Kobalava Z, Vida-Simiti L, Flather M, Shimokawa H, Ogawa H, Dellborg M, Rossi PRF, Troquay RPT,

Libby P, Glynn RJ. Antiinflammatory therapy with canakinumab for atherosclerotic disease. *N Engl J Med* 2017;**377**:1119–1131.
10. Bryan MT, Duckles H, Feng S, Hsiao ST, Kim HR, Serbanovic-Canic J, Evans PC. Mechanoresponsive networks controlling vascular inflammation. *Arterioscler Thromb Vasc Biol* 2014;**34**:2199–2205.
11. Fledderus JO, Boon RA, Volger OL, Hurttila H, Yla-Herttuala S, Pannekoek H, Levonen AL, Horrevoets AJ. KLF2 primes the antioxidant transcription factor Nrf2 for activation in endothelial cells. *Arterioscler Thromb Vasc Biol* 2008;**28**:1339–1346.
12. Zakkar M, Van der Heiden K, Luong Le A, Chaudhury H, Cuhlmann S, Hamdulay SS, Krams R, Edirisinghe I, Rahman I, Carlsen H, Haskard DO, Mason JC, Evans PC. Activation of Nrf2 in endothelial cells protects arteries from exhibiting a proinflammatory state. *Arterioscler Thromb Vasc Biol* 2009;**29**:1851–1857.
13. Van der Heiden K, Cuhlmann S, Luong Le A, Zakkar M, Evans PC. Role of nuclear factor kappaB in cardiovascular health and disease. *Clin Sci* 2010;**118**:593–605.
14. Cuhlmann S, Van der Heiden K, Saliba D, Tremoleda JL, Khalil M, Zakkar M, Chaudhury H, Luong Le A, Mason JC, Udalova I, Gsell W, Jones H, Haskard DO, Krams R, Evans PC. Disturbed blood flow induces RelA expression via c-Jun N-terminal kinase 1: a novel mode of NF-kappaB regulation that promotes arterial inflammation. *Circ Res* 2011;**108**:950–959.
15. Hajra L, Evans AI, Chen M, Hyduk SJ, Collins T, Cybulsky MI. The NF-kappa B signal transduction pathway in aortic endothelial cells is primed for activation in regions predisposed to atherosclerotic lesion formation. *Proc Natl Acad Sci USA* 2000;**97**:9052–9057.
16. Baeyens N, Bandyopadhyay C, Coon BG, Yun S, Schwartz MA. Endothelial fluid shear stress sensing in vascular health and disease. *J Clin Investig* 2016;**126**:821–828.
17. Chatzizisis YS, Coskun AU, Jonas M, Edelman ER, Feldman CL, Stone PH. Role of endothelial shear stress in the natural history of coronary atherosclerosis and vascular remodeling: molecular, cellular, and vascular behavior. *J Am Coll Cardiol* 2007;**49**:2379–2393.
18. Ku DN, Giddens DP, Zarins CK, Glagov S. Pulsatile flow and atherosclerosis in the human carotid bifurcation. Positive correlation between plaque location and low oscillating shear stress. *Arteriosclerosis* 1985;**5**:293–302.
19. Zarins CK, Giddens DP, Bharadvaj BK, Sottiurai VS, Mabon RF, Glagov S. Carotid bifurcation atherosclerosis. Quantitative correlation of plaque localization with flow velocity profiles and wall shear stress. *Circ Res* 1983;**53**:502–514.
20. Wentzel JJ, Janssen E, Vos J, Schuurbiers JC, Krams R, Serruys PW, de Feyter PJ, Slager CJ. Extension of increased atherosclerotic wall thickness into high shear stress regions is associated with loss of compensatory remodeling. *Circulation* 2003;**108**:17–23.
21. Malek AM, Alper SL, Izumo S. Hemodynamic shear stress and its role in atherosclerosis. *JAMA* 1999;**282**:2035–2042.
22. White SJ, Hayes EM, Lehoux S, Jeremy JY, Horrevoets AJ, Newby AC. Characterization of the differential response of endothelial cells exposed to normal and elevated laminar shear stress. *J Cell Physiol* 2011;**226**:2841–2848.
23. Van der Heiden K, Gijsen FJ, Narracott A, Hsiao S, Halliday I, Gunn J, Wentzel JJ, Evans PC. The effects of stenting on shear stress: relevance to endothelial injury and repair. *Cardiovasc Res* 2013;**99**:269–275.
24. Torii R, Tenekecioglu E, Bourantas C, Poon E, Thondapu V, Gijsen F, Sotomi Y, Onuma Y, Barlis P, Ooi ASH, Serruys PW. Five-year follow-up of underexpanded and overexpanded bioresorbable scaffolds: self-correction and impact on shear stress. *EuroIntervention* 2017;**12**:2158–2159.
25. Stone PH, Saito S, Takahashi S, Makita Y, Nakamura S, Kawasaki T, Takahashi A, Katsuki T, Nakamura S, Namiki A, Hirohata A, Matsumura T, Yamazaki S, Yokoi H, Tanaka S, Otsuji S, Yoshimachi F, Honye J, Harwood D, Reitman M, Coskun AU, Papafaklis MI, Feldman CL; PREDICTION Investigators. Prediction of progression of coronary artery disease and clinical outcomes using vascular profiling of endothelial shear stress and arterial plaque characteristics: the PREDICTION Study. *Circulation* 2012;**126**:172–181.
26. Wentzel JJ, Chatzizisis YS, Gijsen FJ, Giannoglou GD, Feldman CL, Stone PH. Endothelial shear stress in the evolution of coronary atherosclerotic plaque and vascular remodelling: current understanding and remaining questions. *Cardiovasc Res* 2012;**96**:234–243.
27. Koskinas KC, Sukhova GK, Baker AB, Papafaklis MI, Chatzizisis YS, Coskun AU, Quillard T, Jonas M, Maynard C, Antoniadis AP, Shi GP, Libby P, Edelman ER, Feldman CL, Stone PH. Thin-capped atheromata with reduced collagen content in pigs develop in coronary arterial regions exposed to persistently low endothelial shear stress. *Arterioscler Thromb Vasc Biol* 2013;**33**:1494–1504.
28. Kubo T, Imanishi T, Takarada S, Kuroi A, Ueno S, Yamano T, Tanimoto T, Matsuo Y, Masho T, Kitabata H, Tsuda K, Tomobuchi Y, Akasaka T. Assessment of culprit lesion morphology in acute myocardial infarction: ability of optical coherence tomography compared with intravascular ultrasound and coronary angioscopy. *J Am Coll Cardiol* 2007;**50**:933–939.
29. Dolan JM, Meng H, Singh S, Paluch R, Kolega J. High fluid shear stress and spatial shear stress gradients affect endothelial proliferation, survival, and alignment. *Ann Biomed Eng* 2011;**39**:1620–1631.
30. Giannopoulos AA, Antoniadis AP, Croce K, Chatzizisis YS. Erosion of thin-cap fibroatheroma in an area of low endothelial shear stress: anatomy and local hemodynamic environment dictate outcomes. *JACC Cardiovasc Interv* 2016;**9**:e77–e78.
31. White SJ, Newby AC, Johnson TW. Endothelial erosion of plaques as a substrate for coronary thrombosis. *Thromb Haemost* 2016;**115**:509–519.
32. Cicha I, Worner A, Urschel K, Beronov K, Goppelt-Struebe M, Verhoeven E, Daniel WG, Garlichs CD. Carotid plaque vulnerability: a positive feedback between hemodynamic and biochemical mechanisms. *Stroke* 2011;**42**:3502–3510.
33. Peiffer V, Sherwin SJ, Weinberg PD. Does low and oscillatory wall shear stress correlate spatially with early atherosclerosis? A systematic review. *Cardiovasc Res* 2013;**99**:242–250.
34. Stone PH, Coskun AU, Kinlay S, Clark ME, Sonka M, Wahle A, Ilegbusi OJ, Yeghiazarians Y, Popma JJ, Orav J, Kuntz RE, Feldman CL. Effect of endothelial shear stress on the progression of coronary artery disease, vascular remodeling, and in-stent restenosis in humans: in vivo 6-month follow-up study. *Circulation* 2003;**108**:438–444.
35. Gijsen FJ, Oortman RM, Wentzel JJ, Schuurbiers JC, Tanabe K, Degertekin M, Ligthart JM, Thury A, de Feyter PJ, Serruys PW, Slager CJ. Usefulness of shear stress pattern in predicting neointima distribution in sirolimus-eluting stents in coronary arteries. *Am J Cardiol* 2003;**92**:1325–1328.
36. Kolandaivelu K, Swaminathan R, Gibson WJ, Kolachalama VB, Nguyen-Ehrenreich KL, Giddings VL, Coleman L, Wong GK, Edelman ER. Stent thrombogenicity early in high-risk interventional settings is driven by stent design and deployment and protected by polymer-drug coatings. *Circulation* 2011;**123**:1400–1409.
37. Rogers C, Tseng DY, Squire JC, Edelman ER. Balloon-artery interactions during stent placement: a finite element analysis approach to pressure, compliance, and stent design as contributors to vascular injury. *Circ Res* 1999;**84**:378–383.
38. Ng J, Bourantas CV, Torii R, Ang HY, Tenekecioglu E, Serruys PW, Foin N. Local hemodynamic forces after stenting: implications on restenosis and Thrombosis. *Arterioscler Thromb Vasc Biol* 2017;**37**:2231–2242.
39. Ruggeri ZM. Platelet adhesion under flow. *Microcirculation* 2009;**16**:58–83.
40. Nesbitt WS, Westein E, Tovar-Lopez FJ, Tolouei E, Mitchell A, Fu J, Carberry J, Fouras A, Jackson SP. A shear gradient-dependent platelet aggregation mechanism drives thrombus formation. *Nat Med* 2009;**15**:665–673.
41. Shankaran H, Alexandridis P, Neelamegham S. Aspects of hydrodynamic shear regulating shear-induced platelet activation and self-association of von Willebrand factor in suspension. *Blood* 2003;**101**:2637–2645.
42. Resnick N, Gimbrone MA Jr. Hemodynamic forces are complex regulators of endothelial gene expression. *FASEB J* 1995;**9**:874–882.
43. Skorczewski T, Erickson LC, Fogelson AL. Platelet motion near a vessel wall or thrombus surface in two-dimensional whole blood simulations. *Biophys J* 2013;**104**:1764–1772.
44. Malek AM, Gibbons GH, Dzau VJ, Izumo S. Fluid shear stress differentially modulates expression of genes encoding basic fibroblast growth factor and platelet-derived growth factor B chain in vascular endothelium. *J Clin Investig* 1993;**92**:2013–2021.
45. Chiu J-J, Chien S. Effects of disturbed flow on vascular endothelium: pathophysiological basis and clinical perspectives. *Physiol Rev* 2011;**91**:327–387.
46. Bourantas CV, Jaffer FA, Gijsen FJ, van Soest G, Madden SP, Courtney BK, Fard AM, Tenekecioglu E, Zeng Y, van der Steen AFW, Emelianov S, Muller J, Stone PH, Marcu L, Tearney GJ, Serruys PW. Hybrid intravascular imaging: recent advances, technical considerations, and current applications in the study of plaque pathophysiology. *Eur Heart J* 2017;**38**:400–412.
47. Tu S, Huang Z, Koning G, Cui K, Reiber JH. A novel three-dimensional quantitative coronary angiography system: in-vivo comparison with intravascular ultrasound for assessing arterial segment length. *Catheter Cardiovasc Interv* 2010;**76**:291–298.
48. Guggenheim N, Dorsaz PA, Doriot PA, Suilen C, Chappuis F, Rutishauser W. 3D determination of the intravascular volume and flow of coronary arteries. *Int J Biomed Comput* 1994;**35**:13–23.
49. Wahle A, Wellnhofer E, Mugaragu I, Saner HU, Oswald H, Fleck E. Assessment of diffuse coronary artery disease by quantitative analysis of coronary morphology based upon 3-D reconstruction from biplane angiograms. *IEEE Trans Med Imaging* 1995;**14**:230–241.
50. Schuurbiers JC, Lopez NG, Ligthart J, Gijsen FJ, Dijkstra J, Serruys PW, Van der Steen AF, Wentzel JJ. In vivo validation of CAAS QCA-3D coronary reconstruction using fusion of angiography and intravascular ultrasound (ANGUS). *Catheter Cardiovasc Interv* 2009;**73**:620–626.
51. Ramcharitar S, Daeman J, Patterson M, van Guens RJ, Boersma E, Serruys PW, van der Giessen WJ. First direct in vivo comparison of two commercially

available three-dimensional quantitative coronary angiography systems. *Catheter Cardiovasc Interv* 2008;**71**:44–50.
52. Toutouzas K, Chatzizisis YS, Riga M, Giannopoulos A, Antoniadis AP, Tu S, Fujino Y, Mitsouras D, Doulaverakis C, Tsampoulatidis I, Koutkias VG, Bouki K, Li Y, Chouvarda I, Cheimariotis G, Maglaveras N, Kompatsiaris I, Nakamura S, Reiber JH, Rybicki F, Karvounis H, Stefanadis C, Tousoulis D, Giannoglou GD. Accurate and reproducible reconstruction of coronary arteries and endothelial shear stress calculation using 3D OCT: comparative study to 3D IVUS and 3D QCA. *Atherosclerosis* 2015;**240**:510–519.
53. Schrauwen JT, Karanasos A, van Ditzhuijzen NS, Aben JP, van der Steen AF, Wentzel JJ, Gijsen FJ. Influence of the accuracy of angiography-based reconstructions on velocity and wall shear stress computations in coronary bifurcations: a phantom study. *PLoS One* 2015;**10**:e0145114.
54. Timmins LH, Suo J, Eshtehardi P, Molony DS, McDaniel MC, Oshinski JN, Giddens DP, Samady H. Comparison of angiographic and IVUS derived coronary geometric reconstructions for evaluation of the association of hemodynamics with coronary artery disease progression. *Int J Cardiovasc Imaging* 2016;**32**:1327–1336.
55. Bourantas CV, Ramasamy A, Karagiannis A, Sakellarios A, Zanchin T, Yamaji K, Ueki Y, Shen X, Fotiadis DI, Michalis LK, Mathur A, Serruys PW, Garcia-Garcia HM, Koskinas K, Torii R, Windecker S, Raber L. Angiographic derived endothelial shear stress: a new predictor of atherosclerotic disease progression. *Eur Heart J Cardiovasc Imaging* 2019;**20**:314–322.
56. Collet C, Onuma Y, Sonck J, Asano T, Vandeloo B, Kornowski R, Tu S, Westra J, Holm NR, Xu B, de Winter RJ, Tijssen JG, Miyazaki Y, Katagiri Y, Tenekecioglu E, Modolo R, Chichareon P, Cosyns B, Schoors D, Roosens B, Lochy S, Argacha JF, van Rosendael A, Bax J, Reiber JHC, Escaned J, De Bruyne B, Wijns W, Serruys PW. Diagnostic performance of angiography-derived fractional flow reserve: a systematic review and Bayesian meta-analysis. *Eur Heart J* 2018;**39**:3314–3321.
57. Morris PD, Ryan D, Morton AC, Lycett R, Lawford PV, Hose DR, Gunn JP. Virtual fractional flow reserve from coronary angiography: modeling the significance of coronary lesions: results from the VIRTU-1 (VIRTUal Fractional Flow Reserve From Coronary Angiography) study. *JACC Cardiovasc Interv* 2013;**6**:149–157.
58. Papafaklis MI, Muramatsu T, Ishibashi Y, Lakkas LS, Nakatani S, Bourantas CV, Ligthart J, Onuma Y, Echavarria-Pinto M, Tsirka G, Kotsia A, Nikas DN, Mogabgab O, van Geuns RJ, Naka KK, Fotiadis DI, Brilakis ES, Garcia-Garcia HM, Escaned J, Zijlstra F, Michalis LK, Serruys PW. Fast virtual functional assessment of intermediate coronary lesions using routine angiographic data and blood flow simulation in humans: comparison with pressure wire—fractional flow reserve. *EuroIntervention* 2014;**10**:574–583.
59. Tu S, Westra J, Yang J, von Birgelen C, Ferrara A, Pellicano M, Nef H, Tebaldi M, Murasato Y, Lansky A, Barbato E, van der Heijden LC, Reiber JH, Holm NR, Wijns W; FAVOR Pilot Trial Study Group. Diagnostic accuracy of fast computational approaches to derive fractional flow reserve from diagnostic coronary angiography: the international multicenter FAVOR pilot study. *JACC Cardiovasc Interv* 2016;**9**:2024–2035.
60. Xu B, Tu S, Qiao S, Qu X, Chen Y, Yang J, Guo L, Sun Z, Li Z, Tian F, Fang W, Chen J, Li W, Guan C, Holm NR, Wijns W, Hu S. Diagnostic accuracy of angiography-based quantitative flow ratio measurements for online assessment of coronary stenosis. *J Am Coll Cardiol* 2017;**70**:3077–3087.
61. van der Giessen AG, Wentzel JJ, Meijboom WB, Mollet NR, van der Steen AF, van de Vosse FN, de Feyter PJ, Gijsen FJ. Plaque and shear stress distribution in human coronary bifurcations: a multislice computed tomography study. *EuroIntervention* 2009;**4**:654–661.
62. Voros S, Rinehart S, Qian Z, Vazquez G, Anderson H, Murrieta L, Wilmer C, Carlson H, Taylor K, Ballard W, Karmpaliotis D, Kalynych A, Brown C 3rd. Prospective validation of standardized, 3-dimensional, quantitative coronary computed tomographic plaque measurements using radiofrequency backscatter intravascular ultrasound as reference standard in intermediate coronary arterial lesions: results from the ATLANTA (assessment of tissue characteristics, lesion morphology, and hemodynamics by angiography with fractional flow reserve, intravascular ultrasound and virtual histology, and noninvasive computed tomography in atherosclerotic plaques) I study. *JACC Cardiovasc Interv* 2011;**4**:198–208.
63. Maurovich-Horvat P, Schlett CL, Alkadhi H, Nakano M, Stolzmann P, Vorpahl M, Scheffel H, Tanaka A, Warger WC 2nd, Maehara A, Ma S, Kriegel MF, Kaple RK, Seifarth H, Bamberg F, Mintz GS, Tearney GJ, Virmani R, Hoffmann U. Differentiation of early from advanced coronary atherosclerotic lesions: systematic comparison of CT, intravascular US, and optical frequency domain imaging with histopathologic examination in ex vivo human hearts. *Radiology* 2012;**265**:393–401.
64. Park JB, Choi G, Chun EJ, Kim HJ, Park J, Jung JH, Lee MH, Otake H, Doh JH, Nam CW, Shin ES, De Bruyne B, Taylor CA, Koo BK. Computational fluid dynamic measures of wall shear stress are related to coronary lesion characteristics. *Heart* 2016;**102**:1655–1661.
65. Sakellarios A, Bourantas CV, Papadopoulou SL, Tsirka Z, de Vries T, Kitslaar PH, Girasis C, Naka KK, Fotiadis DI, Veldhof S, Stone GW, Reiber JH, Michalis LK, Serruys PW, de Feyter PJ, Garcia-Garcia HM. Prediction of atherosclerotic disease progression using LDL transport modelling: a serial computed tomographic coronary angiographic study. *Eur Heart J Cardiovasc Imaging* 2017;**18**:11–18.
66. Bourantas CV, Papadopoulou SL, Serruys PW, Sakellarios A, Kitslaar PH, Bizopoulos P, Girasis C, Zhang YJ, de Vries T, Boersma E, Papafaklis MI, Naka KK, Fotiadis DI, Stone GW, Reiber JH, Michalis LK, de Feyter PJ, Garcia-Garcia HM. Noninvasive prediction of atherosclerotic progression: the PROSPECT-MSCT study. *JACC Cardiovasc Imaging* 2016;**9**:1009–1011.
67. Slager CJ, Wentzel JJ, Schuurbiers JC, Oomen JA, Kloet J, Krams R, von Birgelen C, van der Giessen WJ, Serruys PW, de Feyter PJ. True 3-dimensional reconstruction of coronary arteries in patients by fusion of angiography and IVUS (ANGUS) and its quantitative validation. *Circulation* 2000;**102**:511–516.
68. Wahle A, Prause PM, DeJong SC, Sonka M. Geometrically correct 3-D reconstruction of intravascular ultrasound images by fusion with biplane angiography–methods and validation. *IEEE Trans Med Imaging* 1999;**18**:686–699.
69. Bourantas CV, Papafaklis MI, Athanasiou L, Kalatzis FG, Naka KK, Siogkas PK, Takahashi S, Saito S, Fotiadis DI, Feldman CL, Stone PH, Michalis LK. A new methodology for accurate 3-dimensional coronary artery reconstruction using routine intravascular ultrasound and angiographic data: implications for widespread assessment of endothelial shear stress in humans. *EuroIntervention* 2013;**9**:582–593.
70. Papafaklis MI, Bourantas CV, Yonetsu T, Vergallo R, Kotsia A, Nakatani S, Lakkas LS, Athanasiou LS, Naka KK, Fotiadis DI, Feldman CL, Stone PH, Serruys PW, Jang IK, Michalis LK. Anatomically correct three-dimensional coronary artery reconstruction using frequency domain optical coherence tomographic and angiographic data: head-to-head comparison with intravascular ultrasound for endothelial shear stress assessment in humans. *EuroIntervention* 2015;**11**:407–415.
71. van der Giessen AG, Schaap M, Gijsen FJ, Groen HC, van Walsum T, Mollet NR, Dijkstra J, van de Vosse FN, Niessen WJ, de Feyter PJ, van der Steen AF, Wentzel JJ. 3D fusion of intravascular ultrasound and coronary computed tomography for in-vivo wall shear stress analysis: a feasibility study. *Int J Cardiovasc Imaging* 2010;**26**:781–796.
72. Bourantas CV, Kourtis IC, Plissiti ME, Fotiadis DI, Katsouras CS, Papafaklis MI, Michalis LK. A method for 3D reconstruction of coronary arteries using biplane angiography and intravascular ultrasound images. *Comput Med Imaging Graph* 2005;**29**:597–606.
73. Samady H, Eshtehardi P, McDaniel MC, Suo J, Dhawan SS, Maynard C, Timmins LH, Quyyumi AA, Giddens DP. Coronary artery wall shear stress is associated with progression and transformation of atherosclerotic plaque and arterial remodeling in patients with coronary artery disease. *Circulation* 2011;**124**:779–788.
74. Guo X, Giddens DP, Molony D, Yang C, Samady H, Zheng J, Mintz GS, Maehara A, Wang L, Pei X, Li ZY, Tang D. Combining IVUS and optical coherence tomography for more accurate coronary cap thickness quantification and stress/strain calculations: a patient-specific three-dimensional fluid-structure interaction modeling approach. *J Biomech Eng* 2018;**140**:041005.
75. Wentzel JJ, van der Giessen AG, Garg S, Schultz C, Mastik F, Gijsen FJ, Serruys PW, van der Steen AF, Regar E. In vivo 3D distribution of lipid-core plaque in human coronary artery as assessed by fusion of near infrared spectroscopy-intravascular ultrasound and multislice computed tomography scan. *Circ Cardiovasc Imaging* 2010;**3**:e6–e7.
76. Puri R, Madder RD, Madden SP, Sum ST, Wolski K, Muller JE, Andrews J, King KL, Kataoka Y, Uno K, Kapadia SR, Tuzcu EM, Nissen SE, Virmani R, Maehara A, Mintz GS, Nicholls SJ. Near-infrared spectroscopy enhances intravascular ultrasound assessment of vulnerable coronary plaque: a combined pathological and in vivo study. *Arterioscler Thromb Vasc Biol* 2015;**35**:2423–2431.
77. Tearney GJ, Regar E, Akasaka T, Adriaenssens T, Barlis P, Bezerra HG, Bouma B, Bruining N, Cho J-M, Chowdhary S, Costa MA, de Silva R, Dijkstra J, Di Mario C, Dudeck D, Falk E, Feldman MD, Fitzgerald P, Garcia H, Gonzalo N, Granada JF, Guagliumi G, Holm NR, Honda Y, Ikeno F, Kawasaki M, Kochman J, Koltowski L, Kubo T, Kume T, Kyono H, Lam CCS, Lamouche G, Lee DP, Leon MB, Maehara A, Manfrini O, Mintz GS, Mizuno K, Morel M-A, Nadkarni S, Okura H, Otake H, Pietrasik A, Prati F, Räber L, Radu MD, Rieber J, Riga M, Rollins A, Rosenberg M, Sirbu V, Serruys PWJC, Shimada K, Shinke T, Shite J, Siegel E, Sonada S, Suter M, Takarada S, Tanaka A, Terashima M, Troels T, Uemura S, Ughi GJ, van Beusekom HMM, van der Steen AFW, van Es G-A, van Soest G, Virmani R, Waxman S, Weissman NJ, Weisz G. Consensus standards for acquisition, measurement, and reporting of intravascular optical coherence tomography studies: a report from the International Working Group for

Intravascular Optical Coherence Tomography Standardization and Validation. *J Am Coll Cardiol* 2012;**59**:1058–1072.
78. Koskinas KC, Chatzizisis YS, Antoniadis AP, Giannoglou GD. Role of endothelial shear stress in stent restenosis and thrombosis: pathophysiologic mechanisms and implications for clinical translation. *J Am Coll Cardiol* 2012;**59**:1337–1349.
79. Bourantas CV, Papafaklis MI, Lakkas L, Sakellarios A, Onuma Y, Zhang YJ, Muramatsu T, Diletti R, Bizopoulos P, Kalatzis F, Naka KK, Fotiadis DI, Wang J, Garcia Garcia HM, Kimura T, Michalis LK, Serruys PW. Fusion of optical coherence tomographic and angiographic data for more accurate evaluation of the endothelial shear stress patterns and neointimal distribution after bioresorbable scaffold implantation: comparison with intravascular ultrasound-derived reconstructions. *Int J Cardiovasc Imaging* 2014;**30**:485–494.
80. Thondapu V, Bourantas CV, Foin N, Jang IK, Serruys PW, Barlis P. Biomechanical stress in coronary atherosclerosis: emerging insights from computational modelling. *Eur Heart J* 2017;**38**:81–92.
81. Torii R, Wood NB, Hadjiloizou N, Dowsey AW, Wright AR, Hughes AD, Davies J, Francis DP, Mayet J, Yang GZ, Thom SAM, Xu XY. Fluid-structure interaction analysis of a patient-specific right coronary artery with physiological velocity and pressure waveforms. *Commun Numer Methods Eng* 2009;**25**:565–580.
82. Yang C, Bach RG, Zheng J, Naqa IE, Woodard PK, Teng Z, Billiar K, Tang D. In vivo IVUS-based 3-D fluid-structure interaction models with cyclic bending and anisotropic vessel properties for human atherosclerotic coronary plaque mechanical analysis. *IEEE Trans Biomed Eng* 2009;**56**:2420–2428.
83. Barlis P, Poon EK, Thondapu V, Grundeken MJ, Tu S, Hayat U, Ooi A, Moore S, Tenekecioglu E, Wykrzykowska JJ, Serruys PW. Reversal of flow between serial bifurcation lesions: insights from computational fluid dynamic analysis in a population-based phantom model. *EuroIntervention* 2015;**11**:e1–e3.
84. Manbachi A, Hoi Y, Wasserman BA, Lakatta EG, Steinman DA. On the shape of the common carotid artery with implications for blood velocity profiles. *Physiol Meas* 2011;**32**:1885–1897.
85. Boutsianis E, Dave H, Frauenfelder T, Poulikakos D, Wildermuth S, Turina M, Ventikos Y, Zund G. Computational simulation of intracoronary flow based on real coronary geometry. *Eur J Cardiothorac Surg* 2004;**26**:248–256.
86. Tu S, Holm NR, Koning G, Maeng M, Reiber JH. The impact of acquisition angle differences on three-dimensional quantitative coronary angiography. *Catheter Cardiovasc Interv* 2011;**78**:214–222.
87. Vani A, Underberg JA. Lowering LDL-cholesterol and CV benefits: is there a limit to how low LDL-C needs to be for optimal health benefits? *Clin Pharmacol Ther* 2018;**104**:290–296.
88. Karanasos A, van der Sijde JN, Ligthart J, Witberg K, Regar E. Utility of optical coherence tomography imaging with angiographic co-registration for the guidance of percutaneous coronary intervention. *Radcliffe Cardiol* 2015;1–7. https://www.radcliffecardiology.com/articles/optical-CT-angiographic-PCI.
89. Li Y, Gutiérrez-Chico JL, Holm NR, Yang W, Hebsgaard L, Christiansen EH, Mæng M, Lassen JF, Yan F, Reiber JHC, Tu S. Impact of side branch modeling on computation of endothelial shear stress in coronary artery disease: coronary tree reconstruction by fusion of 3D angiography and OCT. *J Am Coll Cardiol* 2015;**66**:125–135.
90. Dodge JT Jr, Rizzo M, Nykiel M, Altmann J, Hobkirk K, Brennan M, Gibson CM. Impact of injection rate on the Thrombolysis in Myocardial Infarction (TIMI) trial frame count. *Am J Cardiol* 1998;**81**:1268–1270.
91. Kurata A, Kono A, Sakamoto T, Kido T, Mochizuki T, Higashino H, Abe M, Coenen A, Saru-Chelu RG, de Feyter PJ, Krestin GP, Nieman K. Quantification of the myocardial area at risk using coronary CT angiography and Voronoi algorithm-based myocardial segmentation. *Eur Radiol* 2015;**25**:49–57.
92. Coskun AU, Yeghiazarians Y, Kinlay S, Clark ME, Ilegbusi OJ, Wahle A, Sonka M, Popma JJ, Kuntz RE, Feldman CL, Stone PH. Reproducibility of coronary lumen, plaque, and vessel wall reconstruction and of endothelial shear stress measurements in vivo in humans. *Catheter Cardiovasc Interv* 2003;**60**:67–78.
93. Tanedo JS, Kelly RF, Marquez M, Burns DE, Klein LW, Costanzo MR, Parrillo JE, Hollenberg SM. Assessing coronary blood flow dynamics with the TIMI frame count method: comparison with simultaneous intracoronary Doppler and ultrasound. *Catheter Cardiovasc Interv* 2001;**53**:459–463.
94. Murray CD. The physiological principle of minimum work: I. The vascular system and the cost of blood volume. *Proc Natl Acad Sci USA* 1926;**12**:207–214.
95. Zhou Y, Kassab GS, Molloi S. In vivo validation of the design rules of the coronary arteries and their application in the assessment of diffuse disease. *Phys Med Biol* 2002;**47**:977–993.
96. Kassab GS. Scaling laws of vascular trees: of form and function. *Am J Physiol Heart Circ Physiol* 2006;**290**:H894–H903.
97. Rossi A, Merkus D, Klotz E, Mollet N, de Feyter PJ, Krestin GP. Stress myocardial perfusion imaging with multidetector CT. *Radiology* 2014;**270**:25–45.
98. Schrauwen JTC, Coenen A, Kurata A, Wentzel JJ, van der Steen AFW, Nieman K, Gijsen F. Functional and anatomical measures for outflow boundary conditions in atherosclerotic coronary bifurcations. *J Biomech* 2016;**49**:2127–2134.
99. Schrauwen JTC, Schwarz JCV, Wentzel JJ, van der Steen AFW, Siebes M, Gijsen F. The impact of scaled boundary conditions on wall shear stress computations in atherosclerotic human coronary bifurcations. *Am J Physiol Heart Circ Physiol* 2016;**310**:H1304–H1312.
100. Tenekecioglu E, Poon EKW, Collet C, Thondapu V, Torii R, Bourantas CV, Zeng YP, Onuma Y, Ooi ASH, Serruys PW, Barlis P. The nidus for possible thrombus formation insight from the microenvironment of bioresorbable vascular scaffold. *JACC Cardiovasc Interv* 2016;**9**:2167–2168.
101. Davies JE, Whinnett ZI, Francis DP, Manisty CH, Aguado-Sierra J, Willson K, Foale RA, Malik IS, Hughes AD, Parker KH, Mayet J. Evidence of a dominant backward-propagating "suction" wave responsible for diastolic coronary filling in humans, attenuated in left ventricular hypertrophy. *Circulation* 2006;**113**:1768–1778.
102. Hadjiloizou N, Davies JE, Malik IS, Aguado-Sierra J, Willson K, Foale RA, Parker KH, Hughes AD, Francis DP, Mayet J. Differences in cardiac microcirculatory wave patterns between the proximal left mainstem and proximal right coronary artery. *Am J Physiol Heart Circ Physiol* 2008;**295**:H1198–H1205.
103. Westerhof N, Lankhaar JW, Westerhof BE. The arterial windkessel. *Med Biol Eng Comput* 2009;**47**:131–141.
104. Kim HJ, Vignon-Clementel IE, Figueroa CA, LaDisa JF, Jansen KE, Feinstein JA, Taylor CA. On coupling a lumped parameter heart model and a three-dimensional finite element aorta model. *Ann Biomed Eng* 2009;**37**:2153–2169.
105. Chien S, Usami S, Dellenback RJ, Gregersen MI. Shear-dependent deformation of erythrocytes in rheology of human blood. *Am J Physiol* 1970;**219**:136–142.
106. Du VX, Huskens D, Maas C, Al Dieri R, de Groot PG, de Laat B. New insights into the role of erythrocytes in thrombus formation. *Semin Thromb Hemost* 2014;**40**:72–80.
107. Sherwood JM, Kaliviotis E, Dusting J, Balabani S. Hematocrit, viscosity and velocity distributions of aggregating and non-aggregating blood in a bifurcating microchannel. *Biomech Model Mechanobiol* 2014;**13**:259–273.
108. Ku DN. Blood flow in arteries. *Annu Rev Fluid Mech* 1997;**29**:399–434.
109. Boyd J, Buick JM, Green S. Analysis of the Casson and Carreau-Yasuda non-Newtonian blood models in steady and oscillatory flows using the lattice Boltzmann method. *Phys Fluids* 2007;**19**:093103, 1–14.
110. Quemada D. Rheology of concentrated disperse systems.3. General features of the proposed non-Newtonian model—comparison with experimental-data. *Rheol Acta* 1978;**17**:643–653.
111. Hughes TJR. *The Finite Element Method: Linear Static and Dynamic Finite Element Analysis (Dover Civil and Mechanical Engineering)*. Mineola, NY: Dover Publications; 2000.
112. Anderson JD. *Computational Fluid Dynamics: The Basics with Applications*. New York, NY: McGraw-Hill Education; 1995.
113. Chatzizisis YS, Toutouzas K, Giannopoulos AA, Riga M, Antoniadis AP, Fujinom Y, Mitsouras D, Koutkias VG, Cheimariotis G, Doulaverakis C, Tsampoulatidis I, Chouvarda I, Kompatsiaris I, Nakamura S, Rybicki FJ, Maglaveras N, Tousoulis D, Giannoglou GD. Association of global and local low endothelial shear stress with high-risk plaque using intracoronary 3D optical coherence tomography: introduction of 'shear stress score'. *Eur Heart J Cardiovasc Imaging* 2017;**18**:888–897.
114. Himburg HA, Grzybowski DM, Hazel AL, LaMack JA, Li XM, Friedman MH. Spatial comparison between wall shear stress measures and porcine arterial endothelial permeability. *Am J Physiol Heart Circ Physiol* 2004;**286**:H1916–H1922.
115. Peiffer V, Sherwin SJ, Weinberg PD. Computation in the rabbit aorta of a new metric—the transverse wall shear stress—to quantify the multidirectional character of disturbed blood flow. *J Biomech* 2013;**46**:2651–2658.
116. Foin N, Gutierrez-Chico JL, Nakatani S, Torii R, Bourantas CV, Sen S, Nijjer S, Petraco R, Kousera C, Ghione M, Onuma Y, Garcia-Garcia HM, Francis DP, Wong P, Di Mario C, Davies JE, Serruys PW. Incomplete stent apposition causes high shear flow disturbances and delay in neointimal coverage as a function of strut to wall detachment distance: implications for the management of incomplete stent apposition. *Circ Cardiovasc Interv* 2014;**7**:180–189.
117. Sriram K, Salazar Vazquez BY, Tsai AG, Cabrales P, Intaglietta M, Tartakovsky DM. Autoregulation and mechanotransduction control the arteriolar response to small changes in hematocrit. *Am J Physiol Heart Circ Physiol* 2012;**303**:H1096–H1106.
118. Dupin MM, Halliday I, Care CM. A multi-component lattice Boltzmann scheme: towards the mesoscale simulation of blood flow. *Med Eng Phys* 2006;**28**:13–18.
119. Kruger T, Holmes D, Coveney PV. Deformability-based red blood cell separation in deterministic lateral displacement devices—a simulation study. *Biomicrofluidics* 2014;**8**:054114.
120. Lee TR, Choi M, Kopacz AM, Yun SH, Liu WK, Decuzzi P. On the near-wall accumulation of injectable particles in the microcirculation: smaller is not better. *Sci Rep* 2013;**3**:2079.
121. Ii S, Sugiyama K, Takagi S, Matsumoto Y. A computational blood flow analysis in a capillary vessel including multiple red blood cells and platelets. *J Biomech Sci Eng* 2012;**7**:72–83.

122. Zavodszky G, van Rooij B, Azizi V, Hoekstra A. Cellular level in-silico modeling of blood rheology with an improved material model for red blood cells. *Front Physiol* 2017;**8**:563, 1–14.
123. Thondapu V, Tenekecioglu E, Poon EKW, Collet C, Torii R, Bourantas CV, Chin C, Sotomi Y, Jonker H, Dijkstra J, Revalor E, Gijsen F, Onuma Y, Ooi A, Barlis P, Serruys PW. Endothelial shear stress 5 years after implantation of a coronary bioresorbable scaffold. *Eur Heart J* 2018;**39**:1602–1609.
124. Doddaballapur A, Michalik KM, Manavski Y, Lucas T, Houtkooper RH, You X, Chen W, Zeiher AM, Potente M, Dimmeler S, Boon RA. Laminar shear stress inhibits endothelial cell metabolism via KLF2-mediated repression of PFKFB3. *Arterioscler Thromb Vasc Biol* 2015;**35**:137–145.
125. Eshtehardi P, McDaniel MC, Suo J, Dhawan SS, Timmins LH, Binongo JNG, Golub LJ, Corban MT, Finn AV, Oshinsk JN, Quyyumi AA, Giddens DP, Samady H. Association of coronary wall shear stress with atherosclerotic plaque burden, composition, and distribution in patients with coronary artery disease. *J Am Heart Assoc* 2012;**1**:e002543.
126. Papafaklis MI, Takahashi S, Antoniadis AP, Coskun AU, Tsuda M, Mizuno S, Andreou I, Nakamura S, Makita Y, Hirohata A, Saito S, Feldman CL, Stone PH. Effect of the local hemodynamic environment on the de novo development and progression of eccentric coronary atherosclerosis in humans: insights from PREDICTION. *Atherosclerosis* 2015;**240**:205–211.
127. Costopoulos C, Timmins LH, Huang Y, Hung OY, Molony DS, Brown AJ, Davis EL, Teng Z, Gillard JH, Samady H, Bennett MR. Impact of combined plaque structural stress and wall shear stress on coronary plaque progression, regression, and changes in composition. *Eur Heart J* 2019;doi: 10.1093/eurheartj/ehz132 [Epub ahead of print].
128. Gijsen FJH, Wentzel JJ, Thury A, Mastik F, Schaar JA, Schuurbiers JCH, Slager CJ, van der Giessen W, de Feyter PJ, van der Steen AFW, Serruys PW. Strain distribution over plaques in human coronary arteries relates to shear stress. *Am J Physiol Heart Circ Physiol* 2008;**295**:H1608–H1614.
129. Corban MT, Eshtehardi P, Suo J, McDaniel MC, Timmins LH, Rassoul-Arzrumly E, Maynard C, Mekonnen G, King S 3rd, Quyyumi AA, Giddens DP, Samady H. Combination of plaque burden, wall shear stress, and plaque phenotype has incremental value for prediction of coronary atherosclerotic plaque progression and vulnerability. *Atherosclerosis* 2014;**232**:271–276.
130. Vergallo R, Papafaklis MI, Yonetsu T, Bourantas CV, Andreou I, Wang Z, Fujimoto JG, McNulty I, Lee H, Biasucci LM, Crea F, Feldman CL, Michalis LK, Stone PH, Jang IK. Endothelial shear stress and coronary plaque characteristics in humans: combined frequency-domain optical coherence tomography and computational fluid dynamics study. *Circ Cardiovasc Imaging* 2014;**7**:905–911.
131. Stone PH, Maehara A, Coskun AU, Maynard CC, Zaromytidou M, Siasos G, Andreou I, Fotiadis D, Stefanou K, Papafaklis M, Michalis L, Lansky AJ, Mintz GS, Serruys PW, Feldman CL, Stone GW. Role of low endothelial shear stress and plaque characteristics in the prediction of nonculprit major adverse cardiac events: the PROSPECT study. *JACC Cardiovasc Imaging* 2018;**11**:462–471.
132. Fukumoto Y, Hiro T, Fujii T, Hashimoto G, Fujimura T, Yamada J, Okamura T, Matsuzaki M. Localized elevation of shear stress is related to coronary plaque rupture: a 3-dimensional intravascular ultrasound study with in-vivo color mapping of shear stress distribution. *J Am Coll Cardiol* 2008;**51**:645–650.
133. Gijsen F, van der Giessen A, van der Steen A, Wentzel J. Shear stress and advanced atherosclerosis in human coronary arteries. *J Biomechanics* 2013;**46**:240–247.
134. Bourantas CV, Papafaklis MI, Naka KK, Tsakanikas VD, Lysitsas DN, Alamgir FM, Fotiadis DI, Michalis LK. Fusion of optical coherence tomography and coronary angiography—in vivo assessment of shear stress in plaque rupture. *Int J Cardiol* 2012;**155**:e24–e26.
135. Lee JM, Choi G, Koo BK, Hwang D, Park J, Zhang J, Kim KJ, Tong Y, Kim HJ, Grady L, Doh JH, Nam CW, Shin ES, Cho YS, Choi SY, Chun EJ, Choi JH, Norgaard BL, Christiansen EH, Niemen K, Otake H, Penicka M, de Bruyne B, Kubo T, Akasaka T, Narula J, Douglas PS, Taylor CA, Kim HS. Identification of high-risk plaques destined to cause acute coronary syndrome using coronary computed tomographic angiography and computational fluid dynamics. *JACC Cardiovasc Imaging* 2019;**12**:1032–1043.
136. Kumar A, Thompson EW, Lefieux A, Molony DS, Davis EL, Chand N, Fournier S, Lee HS, Suh J, Sato K, Ko YA, Molloy D, Chandran K, Hosseini H, Gupta S, Milkas A, Gogas B, Chang HJ, Min JK, Fearon WF, Veneziani A, Giddens DP, King SB 3rd, De Bruyne B, Samady H. High coronary shear stress in patients with coronary artery disease predicts myocardial infarction. *J Am Coll Cardiol* 2018;**72**:1926–1935.
137. Koppara T, Cheng Q, Yahagi K, Mori H, Sanchez OD, Feygin J, Wittchow E, Kolodgie FD, Virmani R, Joner M. Thrombogenicity and early vascular healing response in metallic biodegradable polymer-based and fully bioabsorbable drug-eluting stents. *Circ Cardiovasc Interv* 2015;**8**:e002427.
138. Wentzel JJ, Gijsen FJ, Schuurbiers JC, van der Steen AF, Serruys PW. The influence of shear stress on in-stent restenosis and thrombosis. *EuroIntervention* 2008;**4 Suppl C**:C27–C32.
139. Thury A, Wentzel JJ, Vinke RV, Gijsen FJ, Schuurbiers JC, Krams R, de Feyter PJ, Serruys PW, Slager CJ. Images in cardiovascular medicine. Focal in-stent restenosis near step-up: roles of low and oscillating shear stress? *Circulation* 2002;**105**:e185–e187.
140. Wentzel JJ, Krams R, Schuurbiers JC, Oomen JA, Kloet J, van Der Giessen WJ, Serruys PW, Slager CJ. Relationship between neointimal thickness and shear stress after wall stent implantation in human coronary arteries. *Circulation* 2001;**103**:1740–1745.
141. Ueba H, Kawakami M, Yaginuma T. Shear stress as an inhibitor of vascular smooth muscle cell proliferation. Role of transforming growth factor-beta 1 and tissue-type plasminogen activator. *Arterioscler Thromb Vasc Biol* 1997;**17**:1512–1516.
142. Jimenez JM, Davies PF. Hemodynamically driven stent strut design. *Ann Biomed Eng* 2009;**37**:1483–1494.
143. Gogas BD, Yang B, Piccinelli M, Giddens DP, King SB, 3rd, Kereiakes DJ, Ellis SG, Stone GW, Veneziani A, Samady H. Novel 3-dimensional vessel and scaffold reconstruction methodology for the assessment of strut-level wall shear stress after deployment of bioresorbable vascular scaffolds from the ABSORB III imaging substudy. *JACC Cardiovasc Interv* 2016;**9**:501–503.
144. Chan CH, Pieper IL, Fleming S, Friedmann Y, Foster G, Hawkins K, Thornton CA, Kanamarlapudi V. The effect of shear stress on the size, structure, and function of human von Willebrand factor. *Artif Organs* 2014;**38**:741–750.
145. Tenekecioglu E, Sotomi Y, Torii R, Bourantas C, Miyazaki Y, Collet C, Crake T, Su S, Onuma Y, Serruys PW. Strut protrusion and shape impact on endothelial shear stress: insights from pre-clinical study comparing Mirage and Absorb bioresorbable scaffolds. *Int J Cardiovasc Imaging* 2017;**33**:1313–1322.
146. Torii R, Stettler R, Raber L, Zhang YJ, Karanasos A, Dijkstra J, Patel K, Crake T, Hamshere S, Garcia-Garcia HM, Tenekecioglu E, Ozkor M, Baumbach A, Windecker S, Serruys PW, Regar E, Mathur A, Bourantas CV. Implications of the local hemodynamic forces on the formation and destabilization of neoatherosclerotic lesions. *Int J Cardiol* 2018;**272**:7–12.
147. Palmerini T, Biondi-Zoccai G, Della Riva D, Mariani A, Sabate M, Smits PC, Kaiser C, D'Ascenzo F, Frati G, Mancone M, Genereux P, Stone GW. Clinical outcomes with bioabsorbable polymer- versus durable polymer-based drug-eluting and bare-metal stents: evidence from a comprehensive network meta-analysis. *J Am Coll Cardiol* 2014;**63**:299–307.
148. Palmerini T, Benedetto U, Biondi-Zoccai G, Della Riva D, Bacchi-Reggiani L, Smits PC, Vlachojannis GJ, Jensen LO, Christiansen EH, Berencsi K, Valgimigli M, Orlandi C, Petrou M, Rapezzi C, Stone GW. Long-term safety of drug-eluting and bare-metal stents: evidence from a comprehensive network meta-analysis. *J Am Coll Cardiol* 2015;**65**:2496–2507.
149. Morrison TM. *Reporting of Computational Modeling Studies in Medical Device Submission—Guidance for Industry and FDA Staff*. Silver Spring, MD: FDA Regulatory Information; 2016.